Chapter 4. Superconductive state of the matter.

4.0 CL space inside a solid body

The CL space of astronomical bodies and small bodies are discussed in Chapter 10. Here only some features of CL space inside a small body could be mentioned. Any solid body placed in the Earth gravitational field is immersed in the CL space of the Earth, which is in fact a CL space of the Milky way galaxy, modulated by the Earth gravitational field (this issue is discussed in Chapters 10 and 12). The atomic matter of the solid body may partially distort the Earth CL space inside of the solid body volume. The distortion is very weak, because at the level of the elementary particles the Newtonian type of gravitational field is quite smaller in comparison to the IG field between the nodes of the CL space structure.

The distortion in fact depends on the intrinsic matter density included in the volume of the solid body. The intrinsic matter density can be expressed by the **number of prisms** included in some **unite volume.** If using the parameters of the electron's structure (unveiled in Chapter 3) the above highlighted parameters are defined. In the same time the electron structure as a single coil of SOHS could be easily referenced to any helical structure, which is embedded in the elementary particles. The protons and neutrons differ only by their overall shape, because they have one and a same internal structures (comprised of helical structures). It is shown in Chapter 8 (and in the Atlas of Atomic Nuclear structures) that the protons and neutrons in the atomic nuclei are arrange in strict order, while the valence protons have some limited freedom of their spatial positions. It is evident that in a microscale range the density of the intrinsic matter exhibits a complex spatial gradient even inside a homogeneous solid body. Since the intrinsic matter density depends on the chosen scale, we may formulate the following scale ranges:

Case (1): a scale in order of proton core envelope thickness equal to: $2(R_c + r_p) = 0.0074$ (A)

Case (2): a scale in order of the proton width:

$W_p = 0.195$ (A)

Case (3): a scale in order of average internuclear distance (1 to 3) (A)

The scale parameters in cases (1) and (2) are determined in Chapter 6.

The average internuclear distance in case (3) depends on number of factors: a pure metal, an alloy or a chemical composition.

The superconductivity is known as a first and a second type.

- The pure first type of superconductivity appears in solids of metals
- The second type of superconductivity appears in solids of allows and chemical compositions

The properties of both type superconductivity are well known. We will try to provide some physical explanation from a BSM point of view of the matter in a CL space environment.

The atoms in metals of solid aggregation state are closer than the nonmetals in a same state. So the metals will exhibit a stronger first type CL space modulation. The specific gravity of the element in a solid state could serve as a reference parameter of this type of modulation. In the same time solids with a same or close specific gravity may have different arrangement of the atoms in the crystal, for example: the structure of the metals and the alloys. While the atoms in the metal crystal are more uniformly spatially distributed, those in the alloys are not. This provides conditions for a stronger IG gradient inside the solid body, which means a larger modulation of the CL space (or CL space spatial non uniformity).

Now if associating the both types of superconductivity with the Earth CL space modulation inside the solid body we see that:

- The CL space modulation in case (1) is not dependent on the particular element, so this type of modulation could be excluded from the superconductivity considerations.

- The CL space modulation in case (2) may depend of the number of the hadrons (proton or neutron) in the nucleus and their arrangement. **Consequently the case (2) may determine which pure metal may exhibit a first type superconductivity.**

- The CL space modulation in case (3) depends on the nonuniformity in the crystal structure configuration. The nonuniformity is smaller for pure metals and larger for alloys, doped metals or

Copyright © 2001, by S. Sarg

chemical compositions. **Consequently the case (3) might be involved in the conditions for second type superconductivity.**

The proof of the above made conclusions will become apparent from the analysis presented in this chapter.

4.1. Normal and superconductive operational mode of CL node.

The superconductivity, according to BSM, is a state of the solid matter, directly related to the ZPE of the internal CL space. When the conductor is cooled to a very low temperature, the CL domains inside its volume may get lower ZPE than the normal one. This condition is dependable on the internal structure of the material. When approaching the absolute zero we see that different metals have different superconductive temperature. Some metals as gold, silver, copper, do not exhibit superconductivity. The nonuniformity of CL space in the solids means that CL structure exhibits stiffness gradients.

The CL nodes of domains with different stiffness have different value of their return forces and consequently different energy wells. This difference affects also their proper resonance frequency. At normal temperature all domains have a normal ZPE

When the body temperature drops to a very low level the domains with a lower stiffness get a lower value of their ZPE in comparison to domains with a higher stiffness. This is much more relevant for the second type or high temperature superconductors, for which the structural mass gradient is much larger, than for the pure metals. The stiffness is very sensitive to the node distance. Small differences in the node distance (or node density) leads to larger stiffness differences, due to the inverse cubic dependence of the IG forces between the nodes.

The return force dependence and the energy diagram of the CL node, was presented in Chapter 2, but the superconductive (**SC**) state was not discussed in details. Here we present the same diagram, but emphasizing on the SC state.

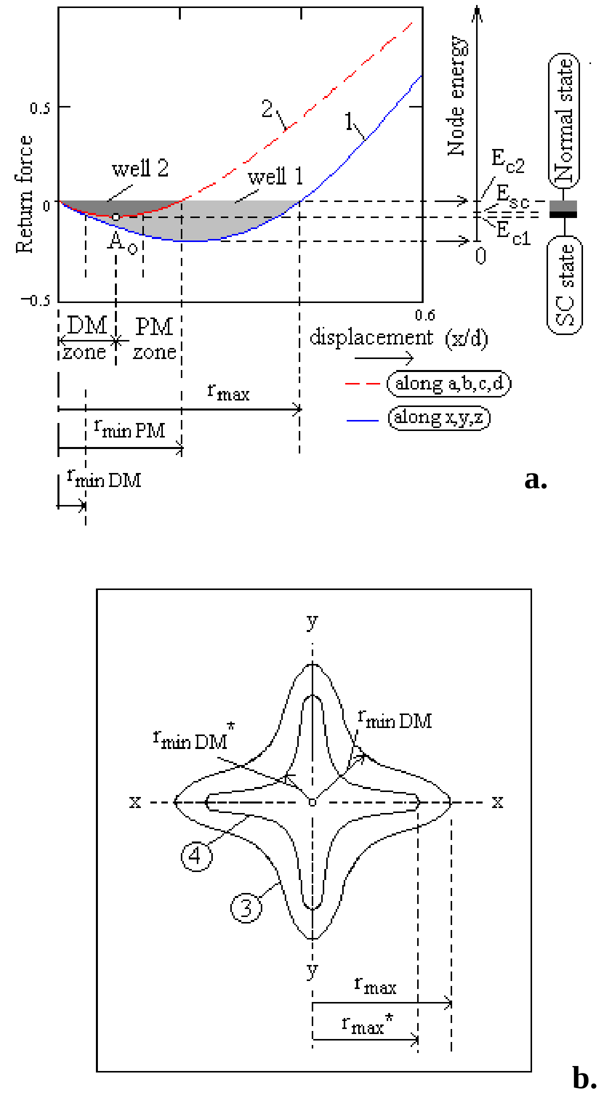

Fig. 4.5
a. Node return forces and energy diagram in function of displacement, b. 2 D projection of the node cycle

Figure 4.5 shows the return forces and the energy diagram as a function of the node displacement with identification of the working energy ranges for a normal and a SC state. The 2D projection of the resonance cycle is given in a different scale in a box below the diagram. The node displacement corresponding to the bumps of the SPM quasisphere is denoted as r_{max}, and this corresponding to the dimples - by r_{min}.

The full well capacity of the node energy is artificially separated into *energy well 1* and *energy well 2.* The *energy well 1* is spatially allocated around *xyz* axes, while the *energy well 2* is allocat-

Copyright © 2001, by S. Sarg

ed around *abcd* axes. The point A_0 is the lowest point of the e*nergy well 1*. The energy scale shown in the right side, is not linear, but showing only the order of the energy levels. The diagram indicates the displacements, corresponding to the r_{max} and r_{min} of the node trace. The radius r_{max} is determined by the curve 1, while r_{min} - by curve 2. We see that both radii are dependent on the level of ZPE down to the critical point A_o, which corresponds to the critical energy level E_{c1}. The level E_{c2} corresponds to a normal ZPE. The radius r_{max} is always defined by the curve 1 for the case of normal and subnormal energy. The same rule, however, is not valid for r_{min}. When the ZPE begins to decrease from E_{c2}, the radius r_{min} initially is determined by the sector of the curve 2 lying in the right side of p. A_0. However, when the energy approaches E_{c1}, the smaller radius may flip to the left side of curve 1. This flipping may occur as a result of an external field influence.

The flipping of r_{min} at a very low energy level may flip the phase of the SPM frequency of the affected domain by a value of π. Then the magnetic filed of this domain could act repulsively to the external magnetic field.

The mentioned effect has direct impact on the external magnetic filed, which tries to penetrate the sample. For r_{min} operated in the left side of p. A_0, the conductor material appears diamagnetic, while in the right side of A_0 it may still appear paramagnetic.

In order to distinguish the node operation of this two cases related with r_{min}, we denote them as a **DM** (diamagnetic) and **PM** (paramagnetic) type of operation. Therefore, p. A_0 separates the diagram in two zones: a **DM zone** and a **PM zone**.

The separation of the node operation in a normal and a superconductor state is a function of the node energy. In fact the normal state should correspond only to one value of the energy level denoted as E_{c2}. The SC state, however, does not begin just below E_{c2}, but is closer to E_{c1}. So between the normal and the SC state, some transition zone with finite energy range should exist. The width of this zone is dependable to some extent on the conductor crystal structure and the atomic mass gradient.

The diamagnetic state is a result of not stabilised resonance frequency. In such case both, the NRM and the SPM vectors are affected. The magnetic filed is very severe disturbed, because it depends on the SPM phase synchronization.

Let to see how the trace shape changes when the ZPE decreases. When approaching SC energy point, the decrease of r_{min} becomes faster than the r_{max}. This changes the shape of the trace from 3 to 4 as shown in the Fig. 4.5. In the same time the NRM and SPM quasispheres are also affected. Their bumps become sharper. The size of the EQ, however, appears restricted by the lower ZPE. As a result of this change, the electrical field around the FOHS may appear stronger, but localised in a smaller space.

Let to see the SPM behaviour in a CL domain, when the ZPE of this domain decreases. At E_{c2} level the SPM frequency is stabilised by the own internal resonance frequency stabilization mechanism. Below this point, this mechanism is lost, but the stabilization could be supported by the neighbouring or the external magnetic field, which is still able to penetrate. This becomes apparent in the FQHE experiments, where an induced quantum effect take place (BSM interpretation). The point E_{c1} corresponds to a bottom critical energy level. **Above this level the spatial rotation of the SPM vector covers the solid angle of 4π. Below the E_{c2} level, however, the SPM vector is not able to cover the full angle of 4π.**

The following conclusion could be made:

- **The point A_0 corresponding to level E_{c1} is very characteristic point for switching the SPM vector behaviour.**

The signature of the characteristic point A_o is identified in the following later analysis of the QHE (Quantum Hall Effect) experiments. It appears at temperature very close to the absolute zero - about 50 mK.

The SC state is above the critical energy level E_{c1}. In order to explain the superconductivity we must consider the CL domains located near the surface and operated in a PM mode. Only in a such mode the SC carrier could interact with the external CL space and create a strong magnetic filed. Then the following question arises: **What kind of interaction is able to keep the located near the surface CL domains in PM type of operation? The answer is: The interaction of the strong magnetic field outside of the superconductor (where the**

Copyright © 2001, by S. Sarg

SPM vector is stabilised) with the oscillating SC carriers. The magnetic field partially penetrates below the surface of the superconductor, where PM zone is created. This is the penetration depth of the superconductor.

The SC carriers are modified versions of the electron system. They are discussed in §4.2.

The penetration depth has an exponential shape, because it is formed by a temperature gradient. The electron and its modified SC configuration, has own self energy in their internal RL(T). So they are automatically attracted in the surface region, where they can exhibit a quantum motion. They are able to keep their normal level of self energy by participating in a quantum motion under control of the external stabilised SPM frequency. The external magnetic field could not pass through the bulk region of the semiconductor, occupied mostly by domains operated in a DM mode. The SPM vectors of these domains (whose frequency is not stabilized) “bounce” the penetrating magnetic lines. This is the **Messner effect.** If applying, however, external filed above some **critical level**, the SC state is destroyed. **In this case the CL nodes, which have operated in the DM zone, forcibly are pressed to operate in the PM zone. The mediator in this interaction is performed by the SC carriers. Their are able to sense the external SMP vector by their oscillations and their affected motion can interact stronger with the CL domains.** If the external field is removed the opposite transition takes place, because the bulk of the superconductor has a lower ZPE.

Let find out what is the sign of the frequency change, when decreasing the normal ZPE and approaching the E_{SC} energy point (see Fig. 4.5), while regarding the CL node as an oscillator, possessing a free running frequency range and stabilized by the mechanism discussed in §2.9.3. It is well known that any stabilised oscillator has a small range of stabilized frequency, characterised by a frequency slop (frequency change from disturbing factors). Outside of this range, the slope is increasing, but without discontinuity. For the oscillating CL node in the range of ZPE between E_{c1} and E_{c2}, there is no reason the first derivative of that slope to change its sign (i. e. there is not discontinuity). Then let find only the sign of the first derivative of this slop. We may obtain this by analysing the thermal properties of the optical materials. When the optical glasses become cooled, their refractive index exhibits a small change. This effect according to BSM is a result of a slight change of the of the SPM frequency in the CL space domain inside the glass. In fact it is affected by a slight reduction of the ZPE of the internal CL space. It is well known, that the 95% of the glasses have a positive change of their refractive index with the temperature. We have to take into account that one additional physical parameter also changes with the temperature - the thermal expansion. The latter change is related with the change of distance between atoms, but we are not sure, could the lattice stiffness be influenced by this. For this reason we must check the temperature trend of the refractive index normalised to the linear expansion coefficient.

$$n/\alpha_T = f\left(\frac{dn}{dT}\right) \tag{4.1}$$

where: n - is the refractive index, α_T - is the thermal expansion coefficient, $(dn/\mathrm{d}T)$ - is the differential change of the refractive index from the temperature

The parameters of 20 glasses were used (the results are not shown here as they can be easily verified). The function (4.7) was plotted and fitted to a robust line. If one and a same wavelength is used, the ratio n/α_T appears very close - mostly in the range 0.30 - 0.31 for 95% of the glasses for the visible range. When including the IR glasses the range becomes larger. **In both case, however, the fitted line is well above the zero.** The glasses showing negative n/α_T gives only 6% contribution, but 5.2% belong to NaCl only. Then, we may conclude with sure, that when the temperature goes down, the corrected refractive index also goes down.

From both options we get one and a same result: **The change of the refractive index, estimated by the parameters of the external CL space, has the same sign as the temperate change.**

As a reference point of the analysis we will consider, the **unchanged node distance**, when the ZPE is decreased. This automatically means, that **the Planck’ constant is unchanged** according to the mass equation. If this was not true, then we will observe a change of a body mass, due to a change of the mass of the particles, but such effect has never been observed.

Copyright © 2001, by S. Sarg

The light velocity as a quantum wave parameter, make a sense only if the quantum conditions are still available, i.e. both, the NRM and the SPM frequencies are stabilised. The change of the refractive index means, a change of the light velocity in the glass. When the glass refractive index goes down, the light velocity, estimated by the external space parameters is increased. Considering the quantum conditions for the first SPM harmonic, the SPM wavelength $\lambda_{SPM}*$, estimated by external space parameters will be increased. If estimated by the number of node distances it will also appear stretched. Then from the energy conservation principle, it follows, that the photon frequency should be decreased because $E = hc/\lambda = h\nu$. The Plank's constant is unchanged, consequently the SPM frequency should be changed. Then, by using up (/|\) and down (\|/) arrows, we may express the signs of the CL space parameters changes as a result of the temperature (T) change.

T \|/ n* \|/ c* /|\ $\lambda_{SPM}*$ /|\ $\nu_{SPM}*$ \|/ (4.2)

where: the parameter in the glass CL space is denoted by *.

The same photon energy in the glass will be stretched in a range, so it will contain a larger number of nodes. The stretched wavelength of the first harmonic will comply to the quantum parameters of CL space inside the glass volume. In fact the stretching is a 3 dimensional. But this could be regarded as a wavelength shift, caused by the changed refractive index, according to the classical interpretation of this phenomenon.

It might be useful to know the direction of the NRM vector frequency change from the temperature. But then a question arises: Is the N_{RQ} value unchanged in respect to the normal state? The answer of this question is not simple. But if we consider, that the energies in both energy wells (well 1 and well 2) are reduced proportionally, then we may accept that N_{RQ} parameter is not affected. Then the change of the NRM frequency will be in the same direction as the SPM frequency change. The same dependence of the NRM frequency from the temperature was also accepted in the node dynamics analysis in Chapter 1, based on logical considerations. This dependence is in agreement, with the accepted model of the conical pendulum. **Consequently, the conical pendulum model is valid for the CL node operating in a PM zone, but not in a DM zone**.

In the further analysis we will rely predominantly on the more confidently determined relations given by Eq. (4.2), allowing to infer the the SPM frequency and the photon wavelength dependence on the temperature. However, when conditions for SPM frequency stabilization appear, we may consider with that the NRM frequency is also stabilised. In SC state such conditions are possible. In the following later analysis of QHE experiments it will be shown that such conditions are actively invoked.

The temperature dependence given by Eq. (4.2) is valid for a normal mode of operation. From the QHE we will see, that the feedback leading to the NRM frequency stabilization is a negative. It is the same type feedback operated in a normal state. Consequently, the feedback leading to a NRM frequency stabilization is of negative type and corresponds to a PM zone, the zone at the left side of point A_0 (Fig. 4.5.a). The slop sign is obviously related with the sign of the feedback, which provides the NRM frequency stabilization. The slop of curve 2 from the left side of A_0 changes the sign. Then the feedback for the nodes operated in the DM zone will become positive. This conclusion is supported by the results from the fractional quantum Hall experiments.

4.2 The electron system configurations in superconductive environments

4.2.1 Electron system in SC state environment. Carriers in SC state of the matter.

The very distinctive features of the electron system from the proton and neutron is that it is composed of three separate helical structures and possesses internal energy, which is kept in its internal rectangular lattices. We may expect, that in domains of normal ZPE, the system always oscillates with small amplitudes. The oscillations create a small alternative magnetic field. This field is directly related to the quantum motion of the electron. The same field, also, assures the symmetrical oscillations of the internal structures in respect to the external one. In other words, this field keeps the internal positron inside the electron's shell. Then we may expect that if the magnetic field is

Copyright © 2001, by S. Sarg

disturbed as a result of abnormal CL space conditions, the electron system could be reconfigured. The most probable reconfiguration is the exiting of the positron out of the electron shell. In the DM zone of SC state, however, the electrical field is stronger and the exiting positron may attach itself externally to the electron shell.

Another mechanism may also favour the exiting of the positron. The normal electron system contains self energy in its internal RL(T)'s. This energy keeps a proper frequencies of the electron system (mostly the first one which is equal to the Compton's frequency) for a finite time. At very low temperature of the superconductor material, the ZPE gradients between domains with different node density are increased. Then small differences between the SPM frequencies of different neighbouring domain may take place. If the moving electron is forced to pass through such domains (by external fields) it may loose the quantum synchronization with the SPM vectors of these domains. Then a low frequency phase difference may occur between the electron proper oscillations and the SPM frequencies of these domains. At large phase biasing, the positron may occur outside of the electron shell. The change of the proper frequency of the positron system from small to large amplitudes (from $3\nu_c$ to $32\nu_c$ respectively) also may contribute to this effect. The process may happens, when the electron is in domains of SC state but operated in PM zone. The conditions for such phase biasing leading to exiting of the positron from electron system are shown in Fig. 9.6

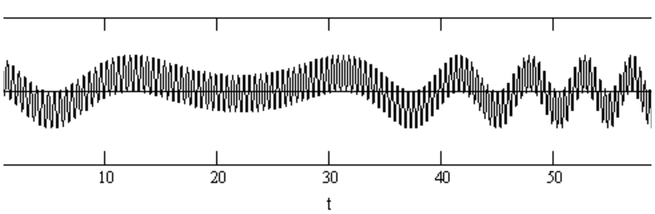

Fig. 4.6
Phase biasing between the electron's oscillations and the SPM frequency of a CL node domain with a lower ZPE leading to exiting of the positron out of the electron's shell (of the electron's helical structure)

The black horizontal line shows the central position of the oscillating positron. We see, that there is number of points at which the positron appears almost outside of the electron's shell. The simulation was provided, by using two close frequencies, one stable for the electron proper frequency and another one with slightly changing sweeping factor, simulating a motion in a zone a CL node proper resonance frequency gradient.

The superconductors of first type are usually metals. However, heavy metals like gold, silver and copper do not exhibit superconductivity. The reason for this is that their crystal structure is pretty uniform, and they have a larger hadron (protons and neutrons) density, which means a larger Intrinsic Matter density. In such conditions, ZPE gradient is relatively small. From the other side, some compounds of heavy and not heavy metals may have CL domains with a larger difference between their stiffness. Then such domains may get a larger ZPE gradient in a comparatively high (in respect to the low temperature superconductivity) temperature. In this conditions, some domains might be in a normal state, while others in a SC state. In this case, the superconductor will have a channel structure. As a result of this, the resistance does not fall so sharply. The Messner effect, however could work even at this conditions, because the magnetic lines need closed paths in order to pass through. A II type superconductors are characterised by such features.

Fig. 4.7.a, and b. show respectively the configuration of the SC electron and the proximity locked external E-field.

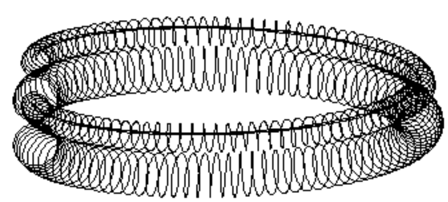

a.

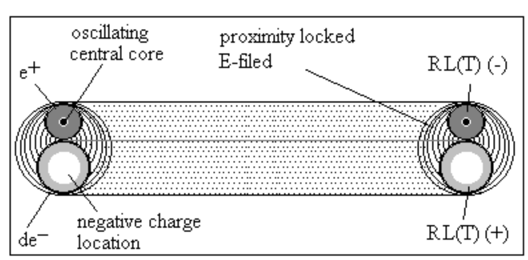

b.

Fig. 4.7. Superconducting electron system and the external proximity locked field. A small gap (not shown) exists between both structures (see the considerations in §6.4.3)

The SC electron distinctive features from the normal electron are the following:

a. **The external electrical field is locked in a proximity.** In the far field the SC electron appears as a neutral particle.

b. **The negative charge is hidden** in the internal region of the twisted mono rectangular lattice of the electron shell. It has openings to the CL space only from both ends.

c. The only oscillation part of the SC electron is the negative central core

When analysing the FQHE experiments we will see, how the SC electron gives its signature as fractional charges of 1/3, 2/3, 4/3, 5/3. The conclusion that the charge appears hidden in the far field is supported also by some experimental observations. J.D.F. Franklin et al. (1995), for example, surprisingly discover in their QHE experiment that, the quasiparticles can tunnel through a barrier.

The intrinsic mass of the positron with its internal lattice appears hidden, when it is inside the electron shell, because the lack of coupling between their IG(CP) lattices, due to the oscillations. Once the positron is external and in a proximity to the electron shell, the motion is absent and the IG(CP) forces are active. They force the E-field lines to get closer and to be connected in proximity. Despite the different external shells radii, the E-fields of the electron and positron are exactly equivalent, because the angular density of their field lines is equivalent. (The Intrinsic Matter difference between the right and left handed prisms is compensated by the CL space). In this conditions the SC electron appears as a neutral in the far field. The hole inside the electron RL(T), however is open and available for the CL nodes. **As a result of this, the existing before the reconfiguration negative charge is transferred to this hole.** There are few reasons supporting this conclusion:

The first one comes from the analysis of the experimental behaviour of the electron during the refurbishing process. If the charge happens to disappear, the CL space should react with an emission of a as in the case of proton - neutron conversion (in this case the β particle according to the BSM is a virtual particle - a reaction of the CL space). **Effect of** β particle emission, however is not detected. This confirms the presented above conclusion.

The second reason comes from the fact that the SC electron is able to be controlled by electrical potential in the superconductor, and it creates magnetic field outside of the superconductor. Consequently it still possesses a guiding feature from the internal negative charge, which is open to the external E-field in both sides of the hole.

In the junction between the superconductor and conductor, the SC electron undergoes refurbishing to a normal electron. **This is the reason for the appearance of the Josephson resistance.** If the charge was missing, the CL space should react as in the neutron - proton conversion, by emission of a β particle. **Such effect is not observed**.

There is a direct observational evidence that the SC electron exhibits a tunnelling effect, passing through a barrier (see quasiparticle tunnelling through a barrier observed by J .D. F. Franklin et all., 1995).

The motion behaviour of the SC electron is different than the normal one. Its interaction with the atoms is greatly reduced. In the same time it still has two important features assuring its quantum type of motion: The first one is the guiding feature of the hidden negative charge, open in both ends of the electron shell. The second one is the oscillation feature of the central core. The second feature assures the quantum motion of the whole system, interacting with the magnetic field of the external space. In SC state, the SC electron naturally prefers to moves in zones near the surface of the superconductor, where the central core interacts with the external magnetic field, which possesses a normal ZPE. We may expect, that the ZPE of this zone of superconductor falls exponentially from the surface to the bulk. Such zone really exists and it is well known under name **a penetration depth.** The internal energy of the positron RL(T) is preserved and serves to support the oscillation of the central core. During a full cycle of the oscillation the part of the end of the negative core moves inside the electron shell hole, occupied now by the negative charge (see Fig. 4.7 (a)) Therefore, the conditions for the central core motion are similar as in the normal electron. **Then we may expect, that the proper frequency of SC electron is the same as the positron-core system in the normal electron.** We will see in the next paragraphs, that this is confirmed by the fractional charge experiments.

Copyright © 2001, by S. Sarg

The SC electron is able to keep its integrity not only in domains in SC state. It can be temporally stable in domains possessing a normal ZPE. Then the motion of the SC electron in a normal ZPE domain will exhibit some resistance, which has to be overcame before the SC electron converts back to a normal electron. This conclusion is confirmed by the experimental data (BSM interpretation). Figure 4.8. shows the temperature dependence of the resistivity of II type superconductor Ba-La-Cu-O for different concentrations of Ba and La.

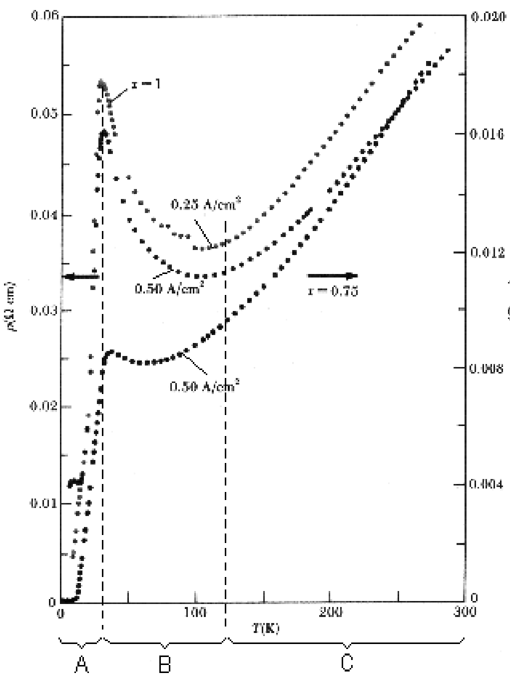

Fig. 4.8
Temperature dependence of the resistivity for II type superconductor based on Ba-La-Cu-O

The temperature scale division in ranges A, B, C is made by BSM interpretation. The range A provides temperature conditions for the CL domains in SC energy state. In the range B, the CL domains approach the normal ZPE level, but the conversion of the SC electron to a normal one is not completed. The SC electrons may temporally survive, when passing domains with normal ZPE. However, their oscillation properties are not optimised for these zones, so they may feel increased resistance. In the same time the abundance of the normal electron is small, because the SC electron is part of the total electron gas. As a result of this, the measured resistance arises. For some concentrations of Ba and La, the domains with a near critical ZPE exist at higher temperature and some SC electrons are still attracted to them. Evidently the balance between the normal domains, the SC domains and the normal electrons leads to a smooth resistance change in the range B. In the temperature range C, all CL domains are with a normal ZPE. The resistance of the SC electron for the back conversion to a normal electron comes from the IG(CP) forces between the degenerated electron and the positron. These forces could be compensated only by the increase of ZPE of the CL nodes. Then more and more CL domains operate in a PM zone. The increased ZPE also removes the restriction on the eccentricity of the EQ quasispheres. In such conditions the electrical and magnetic interactions can overcome the IG(CP) forces. All this factors provide a hysteresis effect in the direction of SC to normal electron conversion process. The hysteresis effect is an important factor, keeping the stability of the SC electron in the SC state. Without such effect the surviving of the SC electron, especially for the II type of superconductors would be a serious problem.

- **The integrity and stability of the SC electron in SC state of the matter is kept by an hysteresis effect.**

The carriers of the SC state are not only single SC electrons. The BSM analysis of the Fractional Quantum Hall experiments (FQHE) unveils the signatures of another configurations of the electron system: - stacked SC electrons. A configuration of two stacked SC electrons is shown in Fig 4.8.A.

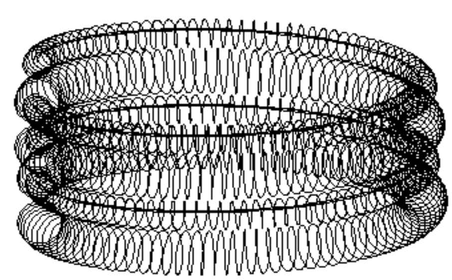

Fig. 4.8.A
Two SC electrons stacked together. The small gaps between the stacked helical structures are not shown , (see the considerations in §6.4.3)

Copyright © 2001, by S. Sarg

The stacked SC system also appears as externally neutral. But it has one distinctive feature in comparison to the single SC electron. One of the positrons is in the middle of the stack. The both ends of its internal core oscillates in domains of hidden electrical charges. In the single SC electron, only one end of the core oscillates in a domain of a hidden electrical charge. The core and the hidden charges are negative, and they repel the core back. One of the hidden negative charges appears between the two central cores. For this reason, the two cores oscillate synchronously and the system exhibits one proper frequency. However this frequency is different than the single SC electron, due to the different oscillation conditions of the cores. In a similar way three or more stacked SC electrons are possible. They have different proper frequencies which signature appears in the BSM analysis of the FQHE experiments. In a system of **n** stacked SC electrons, **(n-1)** positrons are between electron shells. So we may expect that the proper frequency of the stacked SC electron changes with **n**.

The single and stacked SC electrons are the carriers in the superconductivity. One question arises: How the SC electron creates so strong external magnetic field, while its charge is hidden? The answer is:

When the particle is in motion, the proximity locked field of the SC electron is able to generate a magnetic field. This is similar as the neutron case, where the E-filed from its helical structures is locked by the IG forces, but it still exhibits a magnetic moment, when it is in confined motion. The SC electron is attracted in the zone of penetration depth, but this spatial zone has a ZPE gradient. So the SPM frequency (and respectively SPM wavelength) also has a gradient in this zone. Then the boundary quantum conditions of the moving SC electron become not symmetrical, but exhibiting a distorted shape. Fig. 4.9. shows a section of the superconductor near the surface illustrating the boundary conditions of the SC electron for three consecutive subharmonic numbers, n, n+1 and n+2. The ZPE SPM frequency and SPM wavelength are also shown as function of the distance **x** from the surface.

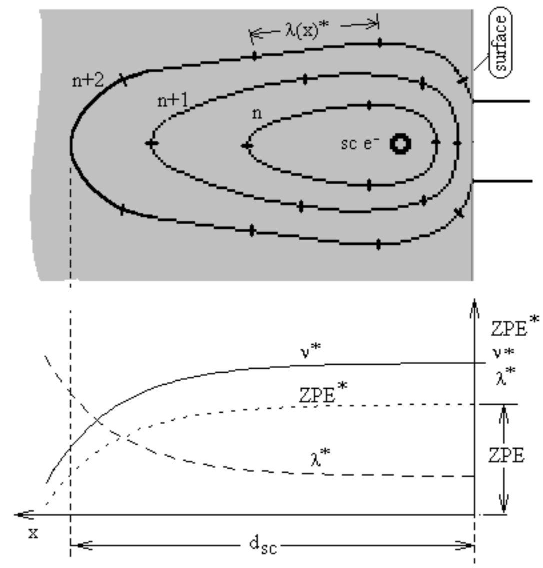

Fig. 4.9
Boundary conditions of the SC electron in the zone of penetration depth. The CL parameters of the superconductor are denoted with *.

The affected CL parameters in SC state are denoted by a "*". We see, that the boundary curves have shapes different than circle due to the ZPE gradient.

The SPM wavelength of in a low ZPE zones is larger than in a normal ZPE zones. The SC electron quantum motion tends to follow the SMP frequency of the local domains through which it moves. Simultaneously its oscillations are influenced by the common magnetic field via direct frequency synchronization. This means the SC carriers with different subharmonic quantum velocity will have different density distribution in the section of the superconductor. Another factor influencing this distribution is the temperature gradient.

If the SC electron following the created quantum conditions tries to move with its optimal confined velocity, its peripheral velocity may reach the limit of the light velocity for this domain (estimated by the number of passed CL nodes per one proper cycle). Therefore, the increasing of $\lambda_{SPM}*$. is constrained. This is apparent from QHE experiments.

The oscillational motion of the SC electrons interacts with the SPM vectors of the low energy

CL nodes. In a SC state of the matter **the "hungry" for energy CL domains do not provide resistance but a complimentary behaviour allowing the SC electron to move almost without resistance.**

The magnetic field of the moving stacked SC electron is a result of the proximity locked external fields between the stacked electron and positron shells. These fields become unlocked only during the quantum screw-like motion (in a similar way as the moving neutron).

Let assuming that some of the induced magnetic lines overpass the surface of the superconductor an pass through the external space (air or vacuum) where CL node SPM frequency is stabilized. In this zone conditions for zero point waves and of magnetic protodomains always exists. Similar conditions does not exist inside the superconductor or they are very diminished. Then the magnetic field from the moving SC electrons will get natural tendency to escape the SC zone and to appear in the outside CL space. At the same time, this tendency will drag the SC charges closer to the surface of the superconductor.

Having in mind that the resistance is very low, the driving voltage is also quite low. This means that the SC electrons may also operate at large subharmonic numbers. In this case their magnetic radius is larger (as for the normal electron discussed in Chapter 2). So it is quite reasonable to expect that the SC electrons have common phase synchronization. This feature may allow the common magnetic field to escape outside of the volume of the superconductor.

After the acquaintance with the nuclear atomic structure (Chapter 8), we will see, that the "positive holes" carriers, which are specific for the semiconductors, can not be carriers in the superconducting state. **Only the single SC electrons and their stacked versions could be the existed charge carriers of the superconductor. This conclusion will become evident, after the analysis of the carriers in the Integer and the Fractional Quantum Hall effect.** This is done in the next two paragraphs.

4.2.2 Proper frequencies of the stacked SC electrons.

In the previous paragraph the reason for the stacked SC electrons proper frequency change was discussed. Here some theoretical explanation of this change will be presented. It was mentioned, that the **proper frequency of the stacked SC electron could be decreased due to the appearance of additional environment for the central core, which oscillates in a spatial domain containing the hidden negative charge (inside of the degenerated electron shell).** We will try to provide some simplified theoretical explanation of such effect.

The stacked electrons may have optimal or subharmonic quantum motion. Let considering only the optimal confined motion (with a first harmonic quantum velocity) of set of SC electrons with stack numbers of 1, 2, 3, 4, 5. Let accepting that their proper frequency as a result of the above discussed effect are respectively:

1/3, 1/5, 1/7, 1/9, 1/11

The above set of fraction numbers in fact appears as a filling factor in the FQHE experiments.

In order to prove the above made conclusion we will provide some analysis of FQHE experiments from the BSM pint of view.

Table 4.1 shows the correspondence between the parameters of the admitted association between the filling factors (well known parameter in FQHE) and the set of the proper frequencies of the stacked SC electrons.

Table 4.1

filling factor	carrier type	ν_{pr}/ν_{SPM}
1/3	- single SC electron	3
1/5	- two stacked SC electrons	5
1/7	- three stacked SC electrons	7
1/9	- four stacked SC electrons	9
1/11	- five stacked SC electrons	11

where: ν_{pr} is the proper frequency of the stacked SC electron and ν_{SPM} is the SPM frequency of the CL node with a normal ZPE.

The negative central core of any consecutive combination of stacked SC electron will get an additional pushing force from the interaction with the hidden negative charge. This will decrease the os-

Copyright © 2001, by S. Sarg

cillation period, which means an increase of the proper frequency. **It is reasonable to expect that when the number of the stacked electron increases, the changed proper frequency of the system will approach a natural exponential shape. Our task is to check this hypothesis.**

From table 4.1 we see that the filling factor set appears as a period of expected frequencies. Then we may estimate the proper frequency change by the period change. The equation of the proper period dependence on the stack number can be written as:

$$i\left(\frac{1}{3}\right) - ix = \frac{1}{2i+1} \qquad (4.3)$$

where: i - is the consecutive stack number, x - is the change of the proper period

Then the change of the proper period is:

$$x = \frac{1}{i}\left(\frac{1}{3} - \frac{1}{2i+1}\right) \qquad (4.4)$$

The grow of x from i is initially larger, but tends to approach a value of 1/3. This is visible from the plot of Eq. (4.4) in Fig. 4.9.A. Two other functions are plotted also, one exponential, given by Eq. (4.5), and one formed of series, given by Eq. (4.6). They both are normalised to a value of 1/3.

$$x_1 = \frac{1}{3}\left[1 - \exp\left(-\frac{ai}{2\pi}\right)\right] \qquad (4.5)$$

where: a = 3

$$x_2 = \frac{1}{3}\left(\sum_{p=1}^{i} \frac{1}{2^p}\right) \qquad (4.6)$$

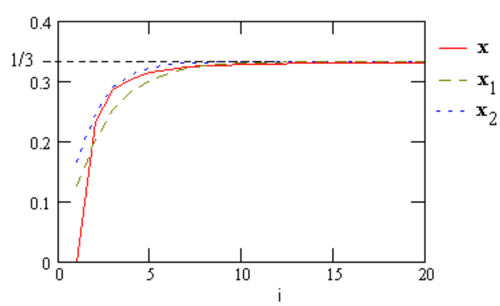

Fig. 4.9.A

The proper period change of the stacked SC electrons in function of the stack number

The factor $a = 3$ in Eq. (4.5) can be considered as a ratio between the proper frequency of the SC electron and the SPM frequency.

We see that the trend of the proper frequency change is less closer to exponential, but much closer to the series given by Eq. (4.6). These series, by the way, have a sequence similar as the subharmonic set 1, 4, 9, 16, valid for a quantum motion with boundary condition of MQ's. Perhaps two factors may influence the proper frequency change: - the changed conditions for the core motion and the new magnetic moment of the stacked structures. From the comparison of electron to muon parameters (having in mind that the electron is a single coil structure, while muon is a multi-coil) we know, that the magnetic moment is inverse proportional to the number of coils.

It is evident that the set 1/3, 1/5, 1/7 exhibits a close trend as the two shown functions. However, one question arises: How the changed proper frequency is possible to take exactly such values with a great accuracy (apparent in the experiments). This answer may be provided by the wavefunction which *Loghline* used for a quasiparticle explanation. This wavefunction obviously is related with some optimum energy balance in quantum space. Then additionally to the above explanation, some physical factor still should exist, allowing the proper frequencies to obtain the exact set values. The possible explanation is the following:

It was discussed in Chapter 2, that the physical dimensions of the FOHS is controlled by the balance of the IG forces given by Eq. (2.8). But small deviation of this balance may affect much stronger the second order helicity and radius. The electron system structures are open FOHS's, whose shape is kept by their internal RL(T). The E-filed of the structure is created by this RL(T). So when the external E-filed is affected due to a lower ZPE, the RL(T) will feel that change. Then it may correct the internal node spacing, that could lead to a small balance change of forces according to Eq. (2.8). As a result of this, the helical step s_e and the radius R_c may undergo a small change, which however is enough to reach the IG forces balance and respectively the exact fractional number corresponding to the observed filling factor.

Copyright © 2001, by S. Sarg

4.3 Integer and Fractional quantum Hall effect, according to the existing so far theories.

The experimental setup and the measured parameters in the integer and the fractional QHE are illustrated by Fig. 4.10.

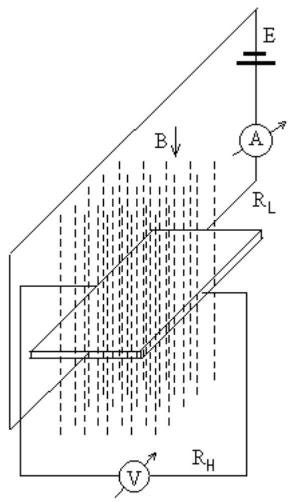

Fig. 4.10
IQHE and FQHE parameter measurements

All experiments of IQHE and FQHE are performed at very low temperature, close to the absolute zero and by applying a strong magnetic field. The sample is usually a very thin GaAs/AlGaAs heterostructure (denoted as a two dimensional), grown in thin layers atop a suitable substrate. The applied magnetic field is normal to the plane of the two dimensional sample.

The charge carriers are driven by the electrical filed applied in X direction. Due to their interaction with the magnetic field, they are deflected and a potential is accumulated in the Y direction. The accumulated potential continues until the created electrostatic force balances the magnetic force on the charge carriers. The equation of balance is: $q\upsilon_d B = qE_H$. Then the generated Hall voltage is:

$$U_H = E_H d = \upsilon_d B d \qquad (4.7)$$

where: E_H is the generated Hall potential per unit length, d - is the width of the strap, B - is the magnetic field, υ_d - is the drift velocity.

Using the kinetic theory, the drift velocity is obtainable. For the semiconductor materials it depends on the temperature.

By changing the strength of the magnetic field the Hall voltage and the longitudinal resistance are changed. The parameters of interest are the Hall resistance R_H and the longitudinal resistance R_L. They are obtainable if the the carrier concentration in the sample is known (a routine technique).

The classical Hall resistance is given by the simple equation,

$$\frac{U_H}{I_d} = R = \frac{B}{nqt} \qquad (4.8)$$

where: *q* is a unit charge, *n* - is the number of carriers, and *t* - is the thickness of the sample.

For given sample the above equation can be normalized to ***t***. The number of carriers, *n*, for the semiconductors depends on the temperature, but for a given temperature Eq. (4.7) gives a linear dependence of the Hall resistance (R) on the magnetic induction (B). In integer and fractional QHE experiments, provided in very thin samples at every low temperature, deviation of linearity appears as plateaus in the Hall resistance, centred about integer or fractional value of the resistance, named a Von Klitzing constant, R_K.

$$R_K = \frac{h}{q^2} = 25813\ \Omega \qquad (4.9)$$

The quantum Hall effect (QHE) is discovered by Klaus and Klitzing in 1980 by observing a two dimensional system at very low temperature and strong magnetic field. Such system exhibits specific conductivity given by

$$\rho = I\left(\frac{e^2}{h}\right), \qquad (4.10)$$

where *I* is a small integer.

A fractional quantum Hall effect (FQHE) was observed, as a big surprise, from number of experiments. In the FQHE, additional plateaus are observed. In order to explain the effect, the concept of degeneracy of the Lanndau level is used. This degeneracy defines a "filling factor" denoted as ν.

$$\nu = nh/qB \qquad (4.11)$$

Then the Hall resistance is modified to the form

$$R_H = \frac{h}{q^2}\frac{1}{\nu} \qquad (4.12)$$

Fig. 4.11 shows the observed Hall and longitudinal resistance for integer and fractional quan-

Copyright © 2001, by S. Sarg

tum Hall effect. (Summury article by J. P. Eisenstein and H. L. Stormer (1990).

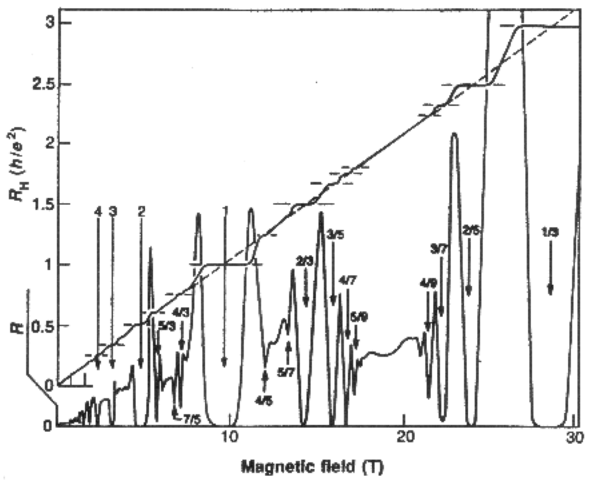

Fig. 4.11
Integer and Fractional quantum Hall effect
(courtesy of J. P. Eisenstein and H. L. Stormer (1990)

From Fig. 4.11 we see, that the Hall resistance R_H obtains plateau for $R_H = R_K$ and for other values, which could be interpreted as integer or fractional charges. They correspond to the Landau filling factors, denoted as ν and defined by Eq. (4.7).

Figure 4.12 shows some other data by D. Tsui et all (1982), where ρ_{xy} denotes the Hall resistance and ρ_{xx} the longitudinal resistance, respectively.

The plots show, also, the temperature dependence of the both resistances that is very useful information for the BSM interpretation.

For IQHE the observed plateaus correspond to the filling factors ν, which are small integers. For FQHE, the plateaus appear for filling factors of: 1/3, 2/3, 4/3, 1/5, 4/5, 1/7 an so on. One of the existing and accepted so far theory is proposed by Laughlin. The Laughlin theory explains the integer and fractional charges as a manybody wavefunction using Landau levels. In additional to the fractional values shown above, however, additional values are also observed: 5/2, 9/2, 11/2 (M.P. Lilly et all., 1998). They can't be explained by the Laughlin quasiparticle theory.

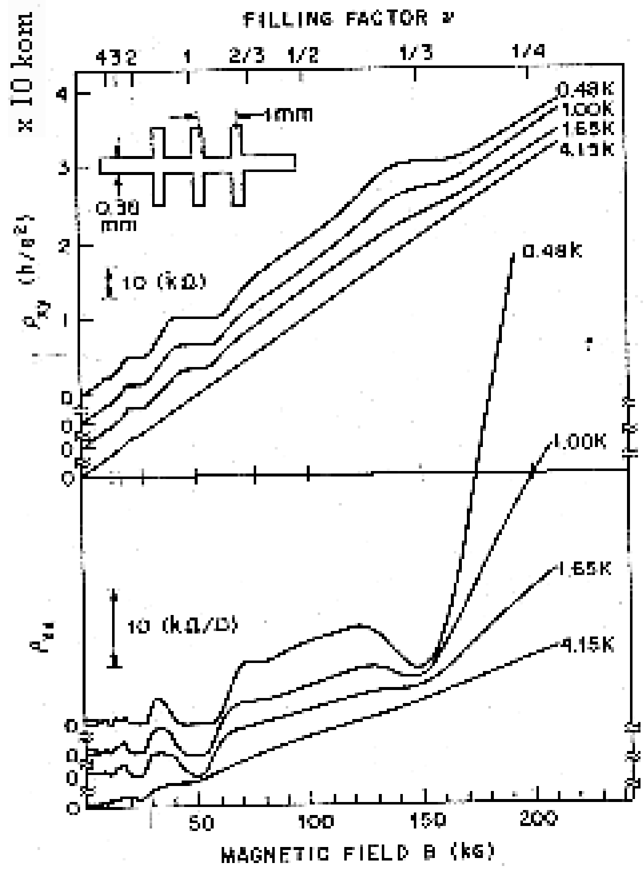

Fig. 4.12
QHE and FQHE (courtesy by D. Tsui et all.)

In 1997 two groups, Israeli (R. de-Picciotto et all. (1997)) and French (L. Saminadayar et all, (1997)) reported shot noise observation corresponding to 1/3e$^-$ fractional charges in two dimensional structures at temperature near to absolute zero. The observed shot noise also put a doubt about the quasiparticle nature of 1/3e$^-$ charge.

Lately in some experiments, Aharonov-Bohm oscillations are clearly observed in the longitudinal resistance for integer and fractional charges. Figure 4.13 shows such data, provided by J. D. F. Franklin et all. 1995. The authors, also, **dis-**

covered, that the quasiparticles can tunnel through a barrier.

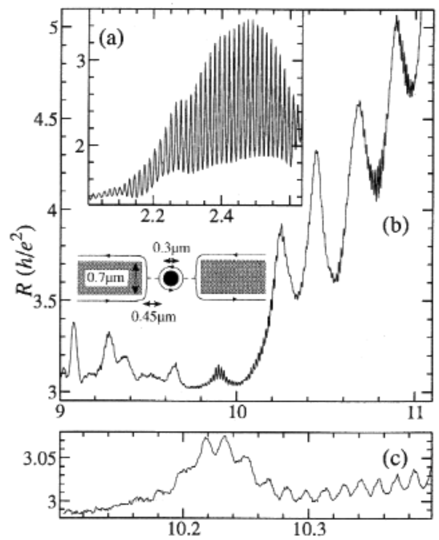

Fig. 4.13
Aharonov-Bohm oscillations for integer and fractional QHE (J.D.F. Franklin et all., (1995)

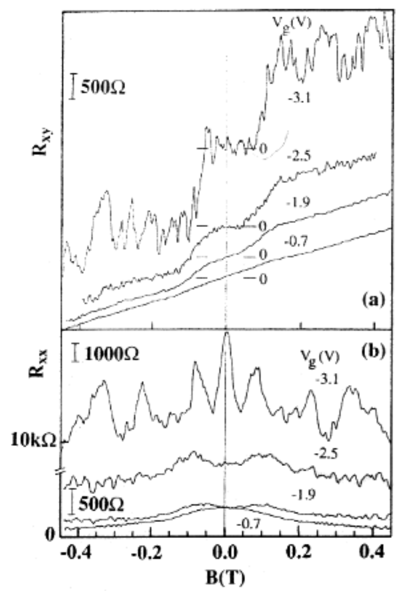

Fig. 4.14
The quenching of the Hall effect near B=0 at T,100 mK (C. Ford et all. (1988)

The accepted from some authors explanation of the Aharonov-Bohm oscillation, as a charge spin separation of the electron in hollon and spinon is also very controversial.

The surprising behaviour of Hall resistance at very low temperature and magnetic field, are subject of extensive and controversial discussions. At temperature below 100 mK and magnetic field approaching zero, the Hall voltage shows large departures from the classical expected value Figure 4.14 shows such observations, provided by C. Ford et all. (1988).

Some other strange phenomena are observed by M. Lilly et all. (1998). Investigating the quasiparticle effects for filling factors of 5/2, 7/2, 9/2, 11/2, 13/2, they observed strong peaks in the longitudinal resistance with not smooth peak top. Then by simply changing the direction of the current through the sample, they observed strong anisotropy of the magnitude of the peaks. Such phenomena has been briefly mentioned by H. L. Stormer et all. (1993) as a puzzling behaviour.

When the FQHE has been examined using a method of surface-acoustic-wave propagation it is observed a strange anomaly of attenuation at $\nu = 1/2$ by E. L. Willet et all. (1990). This phenomenon was observed only at very low temperatures and disappears for temperatures above 700 mK.

Experiments related to the fractional Landau levels but using the cyclotron behaviour of the “quasiparticles” has been provided by Kennedy et all. (1977). They observed a shift in the cyclotron resonance frequency, concomitant with a drastic line width narrowing.

The presented above data a small selection of the experiments in this area.

The BSM theory provides explanation for all of the observed data and phenomena mentioned above.

4.4 QE and FQHE experiments as examples of active control of the light velocity in the sample

4.4.1 General considerations

The quantum Hall effect according to the BSM is very useful phenomenon for investigation of the CL node dynamics at lower ZPE. Our goal is to understand the CL node behaviour at low ZPE.

The benefit from this will be a valuable information about:

- the operation of the SPM vector
- the quantum conditions of CL space
- the oscillation properties of the electron system
- the carriers of SC state of the matter
- the refractive index properties of the superconductors
- the possibility to invoke quantum states and to control the refractive index in the 2D sample (light velocity) in discrete levels

The environment conditions of QHE experiments are very important factors. The most typical conditions at which the experiments are provided are the following:

- The sample is at very low temperature, close to the absolute zero
- The sample is two dimensional, i. e. it contains deposited layer with very small thickness (in the QHE experiments the samples are usually referred as 2D structures)
- Very strong magnetic field is applied

The plane orientation of the layers of 2D sample, in respect to the magnetic field and direction of carrier motion, enhances the condition of their interaction with the magnetic field. Due to the thin multilayer configuration, the refractive index in the layer cross section is not uniform. This reduces the strength of the quantum effect based on the boundary condition of magnetic quasispheres. The influence of other quantum effect described as a "hummer - drill" (HD) effect, becomes now, stronger. This is the effect of the simultaneously moving and oscillating carrier (SC electron). We distinguish two types of interactions due to this effect:

- direct interaction between moving carriers and external magnetic field
- interaction between moving carriers and the quantum conditions in the sample.

Let to pay attention, in first, about the direct interaction between the applied magnetic field and the carriers in the sample. The observation of Aharonov-Bohm oscillations, in the longitudinal resistance (see Fig. 3.14, courtesy of J. D. F. Franklin et all (1995)), make indication **that the carriers are moving in eshellons.** In this case their quantum motions are synchronised, and they are able to be detected. The second benefit from understanding the carrier grouping in eshellons is that their quantum motion could be influenced directly by the strong magnetic field. In the same time the sample SPM frequency is not stabilized. So we have the following oscillators:

- a stabilised SPM frequency of external space, providing the strong magnetic field
- SC electrons, whose proper frequency is stabilized by their internal energy
- a not stabilized SPM frequency of the sample CL space

Now, let see what happens, when changing the magnetic induction. The resistance between the plateaus follows the law of the classical Hall effect. When changing the magnetic field, more or less electrons are forced to deviate from the longitudinal path due to the direct interaction with the external space SPM vector. If the sample was at normal temperature, its SPM vector may create some resistance, but then its frequency is stabilised. If the sample is in a SC state, the node SPM frequency is not stabilized. In this case the number of the magnetic protodomains is decreased. The SPM frequency of the individual domains or nodes may have a phase and frequency dispersion. Then trying to resist the carrier motion their central frequency could be dragged by the forced motion of the carriers. In such case, by changing the magnetic induction we indirectly tune the SPM frequency of the sample. In this process the **carriers serve as a mediator between the external space SPM frequency and the SPM frequency of the sample. They provide the interface connection between the both frequencies. If the sample SPM frequency becomes exactly tuned to a harmonic or subharmonic of the external one, (corrected with the sample refractive index), then the carriers become involved in the quantum motion conditions provided by the both spaces - the external one and this of the sample.** In such case of exact tuning the interface connection becomes stronger. As a result of this, the sample quantum effect gets a positive feedback from the carriers quantum motion, until the phase difference between the external and sample SPM oscillations become zero. The sample SPM frequency gets strong frequency and phase synchronization from the external space SPM frequency. We will call this condition a **syn-**

Copyright © 2001, by S. Sarg

chronized quantum effect. The synchronized quantum effect appears for the three type of the carriers:

- normal electron,
- SC electron
- stacked SC electrons (2, 3, 4, and more stacked electrons)

For any one of the above carriers, the quantum synchronization effect appears when the sample SPM frequency is either equal or a subharmonic of the proper frequency of the carrier. Such synchronization may happen for number of subharmonics for every one of the above mentioned carriers.

The relation between the sample and the external SPM parameters are given by the equation:

$$n_i = \frac{c}{c^*} = \frac{\lambda_{SPM}}{\lambda_{SPM}^*} = \frac{\nu_{SPM}^*}{\nu_{SPM}} \qquad (4.10)$$

where: n_i - is a quantum wave refractive index of the sample, * - denotes the parameters of the sample CL space, wile others are parameters of the external CL space

The Eq. (4.1) should be considered valid not only for optical materials, but for all solids. In such aspect the light velocity appears as a quantum wave velocity, and the quantum wave refractive index should be referenced to the first harmonic of SPM frequency. In the further analysis we will use the term light velocity instead of "quantum wave velocity" for a simplicity.

Let consider, for example, that the magnetic field corresponds exactly to a filling factor $\nu = 1$. At this condition the internal SPM frequency becomes equal to the proper frequency of the normal electron, while the SPM vector of the magnetic field, affected by the sample refractive index, will interact by the frequency: ν_{SPM}/n_i. **When the condition** $\nu_{SPM}^* = \nu_{SPM}/n_i$ **is fulfilled, the electron moving with its optimal rotational frequency (corresponding to the optimal confined velocity) will satisfy simultaneously the external and internal quantum conditions.** If we generalise this condition for carriers with different proper frequencies, for example a single SC electron, **the condition for quantum synchronization becomes:**

$$\nu_{SPM}^* = \frac{\nu_{SPM} p_{pr}}{n_i} \qquad p_{pr} = \nu_{pr}/\nu_{SPM} \qquad (4.11)$$

where: ν_{pr} - is the proper frequency of the carrier, p_{pr} is a proper frequency coefficient

The magnetic field is homogeneous, and the carriers are moving in a direction perpendicular to the magnetic lines. In this conditions, when Eq. (4.11) is fulfilled, a Doppler effect should not be considered. In such conditions, Eq. (4.11) can be extended also for carriers moving with subharmonics, referenced to their proper frequency. Then the quantum synchronization at exact frequency set takes a form:

$$\nu_{SPM}^* = \frac{\nu_{SPM} p_{pr}}{n_i n^*} \qquad (4.12)$$

where: n* - is the subharmonic number of the moving carrier in respect to its proper frequency

It is more convenient to express the quantum synchronization as a function of the sample refractive index. By combining Eq. (4.10) and (4.12) we get:

$$n_i^2 = \frac{p_{pr}}{n^*} \quad \text{or} \quad n_i = \sqrt{\frac{p_{pr}}{n^*}} \qquad (4.13)$$

When applying this analysis for the data from QHE in § 44.5 and § 4.4.5 we will see, that the following relation is valid:

$$p_{pr}/n^* = 1/\nu \qquad (4.14)$$

It appears that, the filling factor ν can be expressed as:

$$\nu = n^*/p_{pr} \qquad (4.15)$$

Then, the sample refractive index expressed by the filling factor is:

$$n_i = \sqrt{1/\nu} \qquad (4.16)$$

Equations. (4.12) to (4.16) are valid for the central position of the plateaus observed in QHE. They, still, do not show the conditions defining the plateau width.

From QHE we see, that the plateau width for the filling factor set 1,2,3,4, and 1/3, 2/3, 3/3, 4/3, 5/3 falls pretty fast with the subharmonic number n^*. The plateau width dependence from the subharmonic number is a result of an effect that we call a **holding condition.** The holding condition characterizes the strength of the quantum effect. This strength depends on the subharmonic number at which the carrier is involved (referenced to the sample SPM frequency). It is largest for n* = 1 and falls exponentially when n* is increasing. It can be

Copyright © 2001, by S. Sarg

illustrated as a holding force between two sliding sinusoids possessing a weight. If the sinusoids have the same period, the holding force is strongest. When the periods are dissimilar the holding force falls rapidly. **We will see from the data that the holding condition appears repeatable for a subharmonic set of different carriers.** We can denote it as a holding function, while the subharmonic number (of the carrier motion in respect to the proper frequency, f(n*)) will be its argument.

The plateau width can be explained if finding a mechanism, that tends to keep the obtained quantum feature of the sample despite the low ZPE level. Such mechanism should provide conditions for keeping the mentioned above feedback when the change of the magnetic flux tries to force the sample SPM frequency to exit from its quantum conditions. The mechanism could be based on a Doppler shift. The latter would not appear between the carrier motion and the applied magnetic field, but between the proper frequency of the carrier and the quantum conditions of the sample.

From the experiment of J.D.F. Franklin et all., (1995), we see, that the carriers are moving in eshellons. We may expect, that the bunch of this eshellons, has a velocity dispersion. Then they will exhibit a range of Doppler shift dispersion. But from number of experiments we see, that the plateau width, if explaining by a Doppler shift due to the axial carrier velocity, will require much larger Doppler shift, than the average drift velocity. In the specific conditions of the QHE experiments, the Doppler effect should be analysed from the point of view of the direct interaction between the PP SPM of the applied magnetic field, propagated in the sample and the hummer drill effect (HD) of the carrier motion.

All the carriers, mentioned above are rotated rings, when they move. They have own proper frequency, and interact with the internal and external quantum conditions, by the HD effect. As a result of this, their rotational velocity obtains an alternative component. This component provides a reference condition for exact comparison between the sample and external SPM frequency with an accuracy up to a portion of the phase. If both frequencies are not exactly equal, a continuous running phase will exist between them. This running phase, regarded as a frequency difference, namely, can contribute a Doppler shift. Having in mind, that electron tangential velocity at optimal confined motion is equal to the light velocity, the running phase may give a very large Doppler shift. It will become evident from the experiments, that the quantum synchronisation effect occurs always for electron tangential velocity in the vicinity of the light velocity estimated by the external space parameters. This is valid for all types of mentioned above carriers.

Let to use the tangential velocity of the electron in order to estimate the Doppler shift from the running phase.

We must not forget that when changing the magnetic flux, we scan the sample SPM frequency, not directly, but via the moving carriers. The local feedback between the sample SPM vector and the carriers provides conditions for a local sample quantum effect. So when trying to push the sample frequency to exit from the quantum hold conditions, the carriers take the frequency discrepancy on themselves, by changing and adjusting the mentioned above running phase. The existing quantum conditions in the external space and in the sample convert the running phase into a Doppler shift. **In such conditions we see, that the Hall effect shows the same resistance, not only for exact frequency value, defined by Eq. (4.12), but in the vicinity of this value, as well. For this reason a quantum plateau in the Hall resistance is observed.**

The direct interaction between the magnetic filed and the rotating electron due to the HD effect is illustrated by Fig. 4.15.

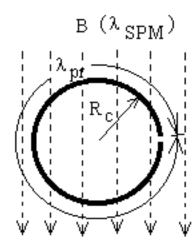

Fig. 4.15. Direct interaction between the external magnetic field and the rotating electron

It is convenient to estimate the Doppler shift by the influence to the external and internal quantum conditions on the tangential velocity of the rotating carrier.

Copyright © 2001, by S. Sarg

The tangential velocity of the rotating electron and all other carriers is given by:

$$\upsilon_t = 2\pi R_c \nu_r \tag{4.16}$$

where: ν_r - is the angular frequency of the rotating electron.

It is evident, that the Doppler shift will contain a pretty large contribution from the difference between the light velocities of the sample and the external space. Let estimate this contribution by using the quantum wave refractive index of the sample, defined by the ratio between the two light velocities. It will be shown from the QHE experiments, that the rotational frequency of the carriers is always in the vicinity of ν_{SPM}/n_i.

Let estimate the frequency range that the Doppler shift could provide for the different combinations, between n^* and p_{pr} parameters, participating in Eq. (4.12). Using the relativistic equation, we estimate the Doppler shift as a dimensionless factor:

$$\Delta\nu = \frac{\Delta\nu_{SPM}^*}{\nu_{SPM}^*} = \sqrt{\frac{\upsilon_{int} - \upsilon_{ext}}{\upsilon_{int} + \upsilon_{ext}}} \tag{4.17}$$

where: υ_{int} - is the tangential velocity confined with the internal quantum interactions, υ_{ext} - is the tangential velocity from the direct interaction with the applied magnetic field.

The velocity υ_{int} has the following dependence from internal quantum conditions:

$$\upsilon_{int} = (c^* p_{pr})/n^* . \tag{4.18}$$

For direct interaction between external SPM frequency and the carrier at first quantum harmonics we get:

$$\upsilon_{ext} = \nu_{SPM}/n_i \tag{4.19}$$

Substituting (4.18) and (4.19) in Eq. (4.17), we get:

$$\Delta\nu = \sqrt{\frac{|1 - n^*/(p_{pr} n_i)|}{1 + n^*/(p_{pr} n_i)}} \tag{4.20}$$

Note: Both υ_{int} and υ_{ext} are estimated by the external space parameters.

The nominator under square root is put in modulus, because the velocity difference can take either positive or minus sign. It comes from the tuning possibility of ν_{SPM^*} by B, (from both sides of the exact quantum synchronization value) from one side, and from different ratio n^*/p_{pr}, from the other.

According to Eq. (4.20), the plateau width for one and a same type of carriers will depend of n* and will decrease when n* is growing. However, the plateau width is not completely determined by Eq. (4.2). From the experiments we see, that the plateau width falls pretty sharp with n*. The plateau width does not depend on a single factor. So if defining a hold function, which defines completely the plateau width, it should take into account the following three factors:

- the Doppler shift, defined by Eq. (4.20)
- the non linear dependence of n_i from B,
- the strength of the direct interactions

let to determine the contribution from the second factor. When analysing the data from QHE we will see, that the $1/\nu$ factor has completely linear dependence of B, so the following relation is valid:

$$1/\nu = k_{sl} B \tag{4.21}$$

where k_{sl} is the coefficient of proportionality (the slop of the fitted line). Then according to Eq. (4.16) we have.

$$n_i = \sqrt{k_{sl} B} \tag{4.21.a}$$

The variation of B will cause a variation of n_i. We can estimated it as a first derivative of n_i from B.

$$\Delta n_i = \frac{1}{2}\sqrt{\frac{k_{sl}}{B}} \tag{4.22}$$

The larger variation of n_i means a lower holding effect. Consequently, the holding contribution should be inverse proportional to Δn_i.

$$1/(\Delta n_i) = 2\sqrt{B/k_{sl}} \tag{4.23}$$

The third factor is the drag momentum in the direct interactions by HD effect. In a first approximation, it could be simulated as a normalised momentum difference between two sliding sinusoids with a frequency ratio, corresponding to a subharmonic number. Analytically, such condition is expressed by the equation:

$$\int_0^{2\pi} [\sin(x) - \sin(n^* x + \varphi)]dx = \frac{\cos(2\pi n^* + \varphi) - \cos(\varphi)}{n^*} \tag{4.24}$$

The solution (4.24) is not defined for integer n*, but is defined for $(n^* + \varepsilon)$, where ε is small enough (for example 0.001). Then we may obtain the solutions for consecutive $(n^* + \varepsilon)$, and normalise them to the value of $n^* = 1$. The obtained function fits excellently to a simple function:

Copyright © 2001, by S. Sarg

$$y = 1/n^* = \eta_{HD} \qquad (4.25)$$

The obtained simple equation (4.25) could be regarded as a quantum efficiency of the HD effect, referenced to the external SPM field.

The quantum efficiency η_{HD} is related to the plateau width.

The contributions from all three factors, presented by Eq. (4.20, (4.23) and (4.25) act simultaneous, so the total frequency shift defining the plateau width should be equal to their product.

$$\Delta\nu = \pm\frac{2a_1}{n^*}\sqrt{\frac{B}{k_{sl}}\left[\frac{|1 - n^*/(p_{pr}n_i)|}{1 + n^*/(p_{pr}n_i)}\right]} \qquad (4.26)$$

where: $\Delta\nu$ - is a normalised plateau width, a_1 is a coefficient of proportionality.

If estimating the plateau width by the range of *B* change, we have.

$$w = a_s(\Delta\nu) \qquad (4.27)$$

The coefficient a_s, takes into account the strength of the interaction.

Eq.uation (4.27) gives closer values of calculated plateau with for single and stacked SC electrons, moving by different subharmonics. It does not give closer values if applied for normal electrons. While in first case, the charge is hidden, in a second one it is not. The reason is that for electron moving with $n^* = 1$, the interaction could be enforced by formation of some boundary conditions of MQ's, as in the normal state of the matter.

The frequency shift in the real case may deviate from Eq. (4.26), because we used idealised case of momentum difference between two sinusoidal sources for the direct interaction between carriers and the magnetic field. While the carrier proper frequency is of sinusoidal type, the bumps of the CL node magnetic quasisphere are not sinusoidal. This will alter the simple interaction function given by Eq. (4.25). But this could give one useful possibility to investigate the shape of the magnetic quasisphere. In the present analysis, we will not go so far, because more factors should be taken into account.

Additional small Doppler shift, that may influence the quantum stabilization, may be contributed by the velocity dispersion between the carrier eshellons. This Doppler shift is convolved with the major Doppler shift, because the eshellon carriers participate in the both interactions simultaneously. This will give a comb like structure of the combined Doppler shift. There is also a threshold level for development of synchronised quantum effect. If the coefficient a_1 is large enough and the threshold level is inside the comb like Doppler shift, oscillations appear in the longitudinal resistance. This oscillations are known as Aharonov-Bohm oscillations. They are experimentally observed (see Fig. 4.13). In many QHE experiments, these type of oscillations are not observable, because, the lack of special conditions, necessary to enhance this effect to a level of detection.

The Aharonov-Bohm oscillations, even undetectable, may play a role in the plateau formation. When changing the magnetic flux, the quantum synchronization effect starts to work before the central point of the plateau is reached. This might be explained by the velocity distribution of the carriers participating in the eshellons. Let suppose, that all electrons in one eshellon have synchronised rotational frequency due to their local HD effect and the interaction with the local protomagnetic domains. Such eshellon may have much stronger direct interaction with the magnetic field. When the Doppler shift from the combined factors satisfies the Eq (4.19), a synchronised quantum effect will be obtained.

The frequency range at which the sample is synchronised is usually lower than its SPM frequency at normal ZPE (not cooled conditions). This is due to the resonance frequency decrease when the temperature approaches the SC state. This explains why all the plateau widths exhibit a same temperature dependence. This is clearly shown by the experimental data provided by D. Tsui et all (1982) (see Fig. 4.12).

As a result of the low temperature SPM frequency shift, the sample's quantum features are also shifted.

The SPM frequency defines the light velocity in the sample. If all quantum features are shifted as a result of cooling, **the sample CL parameters can be identified by the optimal confined motion of the electron**. Then the quantum wave (light) velocity of the sample can be estimated. It may appear, that the quantum refractive index, identified by the internal quantum features gets smaller value than unity for some filling factors. **This is very interesting result, but it appears in the data analysis from the QHE experiments.**

Copyright © 2001, by S. Sarg

Comparing the quantum motion of the electron system in normal ZPE, derived by hydrogen series, with this in the QHE experiments, we see that the allowed levels corresponds to a consecutive subharmonic numbers of: 1, 2, 3, 4, 5. This provides additional confidence and confirmation about the subharmonic set used to describe the quantum motion of the electron system.

From the provided analysis we see, that the quantum Hall experiments give a possibility to scan the SPM frequency of the 2D sample at very low temperatures, by changing the magnetic field. The diagram of the involved interaction processes is illustrated in Fig. 4.16.

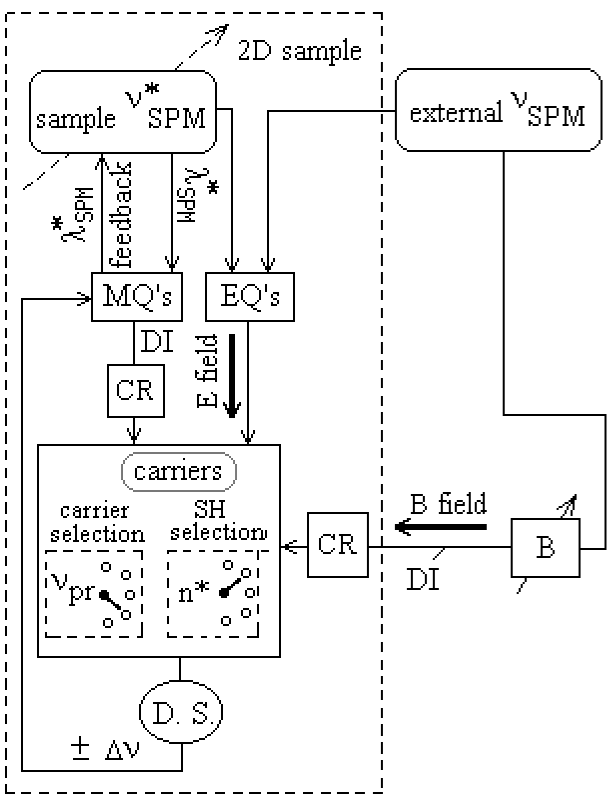

Fig. 4.16
Scanning of the sample SPM frequency in QHE
DI - direct interaction; CR - carrier rotation,
D.S. - Doppler shift; SH - subharmonic (defining the carrier velocity)

Summarizing the synchronised quantum effect, it is useful to emphasize the following features:

- **The allowable stabilization frequencies for the induced quantum effect are determined by the combinations between the proper frequency of the involved carrier $\nu_{SPM}*$, and the subharmonic $n*$ at which the carrier performs a confined motion in the condition of the induced quantum effect.**
- **The quantum wave velocity (respectively the refractive index) is defined only for the points of the induced quantum effect.**
- **In conditions of induced quantum effect, the first derivative of the longitudinal conductance in function of the Doppler shift is negative.**

The third feature is related with the carrier mobility in a confined motion. When the Doppler shift is zero, the strength of the confined motion due to the internal quantum effect has a maximum value and the longitudinal conductance is also maximized. This means, that the sample CL space allows the carriers to move with minimum energy loss. **This feature explains also, why the electrons in the normal state of the matter (at normal ZPE) obtain preferable velocities due to the quantum motion.**

4.4.2 Signature of the electron system in the Integer quantum Hall effect

Let suppose, that we scan B from right to left and approach the plateau of filling factor $\nu = 1$. Due to the finite value of ν_{rot}, the Eq. (4.11) will become satisfied before reaching the exact value of *B* corresponding to the $\nu = 1$. A similar conditions appear, when overpassing the exact value. As a result of this, a plateau appears. It is exactly symmetrical on $\nu = 1$, because the Doppler shift and the holding functions are symmetrical about the plateau centre. When *B* is near the edge of the plateau, less carriers are involved in the quantum stabilization process. Approaching the plateau centre, more carriers are involved. This is consistent with the change of the longitudinal resistance under the plateau. So we see, that for the integer QHE the plateau for $\nu = 1$ is contributed by the normal electron, moving with an optimal confined velocity, estimated by both, the external space and the sample SPM. Consequently, the sample SPM frequency is locked to the value of the external space SPM frequency, divided by the sample refractive index, valid for this point. In the same time the sample SPM frequency, could be smaller that its value at normal ZPE, due to the temperature SPM

Copyright © 2001, by S. Sarg

frequency shift. If estimating the electron velocity by the number of passed nodes per one fundamental time base (Compton time), it will appear closer to the drift velocity, of the sample at normal temperature, corrected by the effect of the temperature SPM frequency shift.

If the scanning magnetic field approaches a value for a filling factor 2, the sample SPM frequency becomes locked to a lower value and gives again a quantum motion conditions. In this case, the sample SPM frequency is half of the external one and its $\lambda_{SPM}*$ is twice longer that the λ_{SPM}. The filling factor 2 corresponds to a quantum motion of the normal electron with a second subharmonic, estimated by the proper frequency (equal to the internal SPM frequency for a normal electron). When estimated by the external SPM frequency the motion again corresponds to a first harmonic.

Consequently we may conclude, that:

- **The quantum signature of the normal electron is provided by the QHE plateaus. When estimated by the external SPM frequency, the quantum motion corresponds to the first harmonic, but when estimated by the proper frequency it appears as a subharmonic. The subharmonic number is equal to the Landau level number.**

Let to use the experimental data provided in the article of J. Eisenstein and H. Stormer, (1990) and shown in Fig. 4.11. The identification of the normal electron signature is shown in Table 4.2. The last column shows the tangential velocity **estimated by the external space parameters** (c - is the light velocity in the external space).

Signature of the normal electron

$p_{pr} = 1$ Table 4.2

Filling factor ν	$n*$	n_i	B [T]	$\upsilon_t = c/n_i$ [km/s]
1	1	1	9.59	c/1
2	2	0.7071	4.79	1.414c
3	3	0.5773	3.14	1.732c
4	4	0.5	2.37	2c

4.4.3 Signature of the SC electron in the FQHE

We found out, that the plateaus for the integer QHE are produced by the normal electron. Let, now, see what is the signature of the SC electron.

The single SC electron has a proper frequency 3 times larger than the Compton frequency: $\nu_{pr} = 3\nu_{SPM}$. Then a similar process will develop, when the B field has a larger value than for $\nu = 1$. In this case the sample SPM frequency gets a value three times higher, than for level one. In this conditions the SC electron gets an optimal confined motion, estimated by the sample SPM parameters and by external space. This corresponds to a level $\nu = 1/3$. In the same time the absolute value of $\nu_{SPM}*$ may be lower that this at normal temperature.

At level 2/3, the SC electron is moving as a second harmonic estimated by its proper frequency, and first harmonic estimated by external SPM frequency (but corrected by n_i.) In a similar way the levels 3/3, 4/3, 5/3, 6/3 correspond to quantum motion at 3, 4, 5, 6 subharmonic, estimated by the proper frequency of the SC electron.

The locking conditions for the single SC electron, according to Eq. (4.13) are given by Table 4.3, where: $n*$ - is the subharmonic number estimated by the carrier proper frequency, $\nu_{SPM}*$, The last column is the tangential velocity, υ_t, estimated by the external space parameters. The frequency ratio between the proper frequency of the SC electron and external SPM frequency ν_{SPM} is $p_{pr} = 3$.

Signature of the single SC electron

$p_{pr} = 3$ **Table 4.3**

Filling factor ν	$n*$	n_i	B [T]	$\upsilon_t = c/n_i$ [km/s]
1/3	1	1.732	28.7	0.577c
2/3	2	1.225	14.3	0.8163c
1	3	1	9.67	1c
4/3	4	0.866	7.14	1.155c
5/3	5	0.7746	5.69	1.291c
2	6	0.7071	4.79	1.414c

We see, that the plateaus at filling factors 1 and 2 are contributed by both, the normal electron and the single SC electron.

Copyright © 2001, by S. Sarg

4.4.4 Signature of the stacked SC electrons

The proper frequencies of the stacked electrons were given in Table 4.1. The signatures of the two and three stacked electrons are shown respectively in Table 4.4, and Table 4.5 The same source of the experimental data is used.

Signature of two stacked SC electrons

$p_{pr} = 5$ **Table 4.3**

Filling factor ν	n^*	n_i	B [T]	$\upsilon_t = c/n_i$ [km/s]
1/5	1			
2/5	2	1.581	23.9	0.633c
3/5	3	1.291	15.9	0.7746c
4/5	4	1.118	11.96	0.8944c
1	5	1	9.59	c
6/5	6	0.8452	6.77	1.183c

Signature of three stacked SC electrons

$p_{pr} = 7$ **Table 4.3**

Filling factor ν	n^*	n_i	B [T]	υ_t [km/s]
1/7	1			
2/7	2			
3/7	3	1.528	22.3	0.6544c
4/4	4	1.323	16.7	0.7558c
5/7	5	1.183	13.36	0.8453c
6/7	6	1	9.59	c

4.4.5 Scanning the sample SPM frequency and invoking a synchronised quantum effect

Without the presence of the electron and its SC configurations, the scanning of the low energy SPM frequency of the sample and the synchronised quantum effect would not be possible.

Fig 4.16 shows a plot of the frequency ratio (ν_{SPM}^*/ν_{SPM}) in function of the magnetic inductance *B*. The data are taken from the Tables 4.2 to 4.5. The carriers are shown as square dots and are connected with a line, showing a linear trend. The notations by the filling factor are shown below the line, while the notations of the identified carriers - above the line. In the right side of the plot, the discrete values of the sample refractive index are show.

While the SPM ratio could be considered as a continuous function, the refractive index is defined only for these discrete values, for which a synchronized quantum effect is possible.

One surprising result of the synchronised quantum effect is that, the refractive index of the sample for filling factor below 1, becomes smaller than unity. This means, that the light velocity in the sample estimated by the external frame is larger than the light velocity in vacuum. This result is a logical, because it corresponds to $\lambda_{SPM}^* > \lambda_{SPM}$, estimated by the external frame parameters. We, may confirm this result, by some analysis of the node dynamics.

It is apparent from the presented plot in Fig. 4.16, that the sample SPM frequency is really scanned, when changing the magnetic flux. If using data for other carriers, corresponding to the stacked SC electrons with larger stacked number, they also lie in the same curve. We see that the dynamical range of the frequency change, form this data is 3.5.

While the sample SPM frequency follows the magnetic flux, the synchronised quantum effect appears, only when Eq. (4.17) is satisfied. These are discrete points in the SPM frequency scale. The quantum light velocity and the refractive index that the sample obtains are defined only for this points. The quantum refractive index scale with its discrete values is shown in the right side of the plot.

Copyright © 2001, by S. Sarg

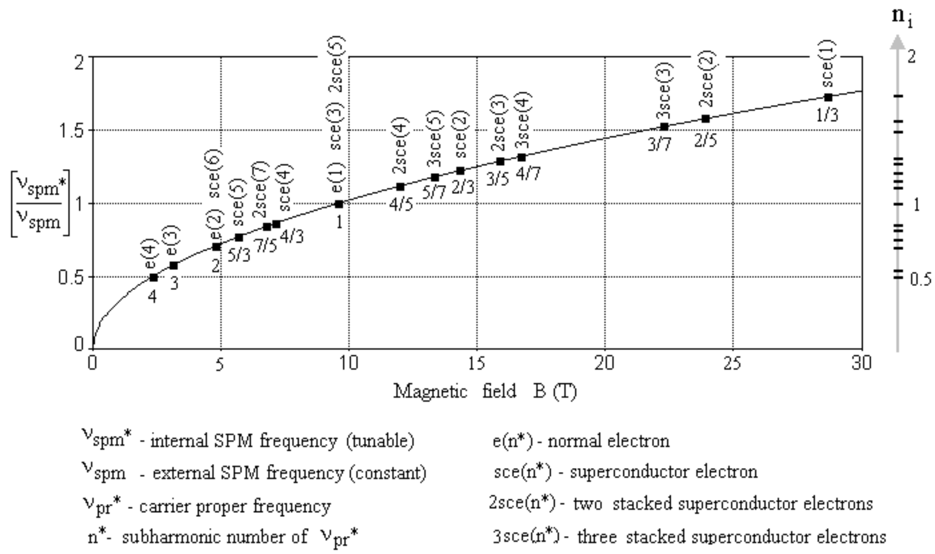

Fig. 4.17

Scanning of SPM frequency in QHE experiments

We see, that the function $n_i = f(B)$ is a discrete function, while $(\nu_{SPM}^*/\nu_{SPM}) = f(B)$ is a continuous one. For simplicity, however, we may use the first function, regarding it as an interpolated function passing through discrete values. In the analysis, we found, that the sample refractive index in function of the filling factor is given by the simple Eq. (4.15)$n_i = \sqrt{1/\nu}$. The argument of this function depends on *B*. We can plot the function $1/\nu = f(B)$ from the same data tables. It is shown in Fig. 4.18, fitted to a robust line. It is perfectly linear with a slop coefficient $k_{sl} = 0.10445$

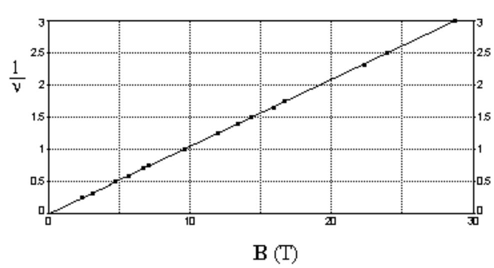

Fig. 4.18

Plotting data from different experiments we get a same linear dependence of $(1/\nu)$ from B, but with different coefficient k_{sl}. Then the following relation is obviously valid:

$$\frac{1}{\nu} = \frac{qB}{nh} = k_{sl}B \qquad (4.28)$$

From Eq. (4.28) we get:

$$: k_{sl} = \frac{q}{nh} \qquad (4.29)$$

where *n* - is the number of carriers.

We see from Eq. (4.29) that the slop of B depends only on the number of carriers, while the unit quantum flux (h/q) is unchanged. There is not evidence, again, that a fractional charge could exist. This in agreement with the accepted rule, for the charge unity.

There is one additional outcome from the function expressed by Eq. (4.28). If we put the plateaus in the plot in Fig. 4.16, they will be parallel to *B* axis as in the Hall resistance plot. In the same time the plateaus indicate the points of the sample SPM frequency stabilization. Then the plot of Eq. (4.28) is very similar to the theoretical plot of the frequency of the conical pendulum in function of the relative displacement x, that was discussed in $2.9.3 and given by Eq. (2.17.f). (Resonance frequency stabilization, Chapter 2). The general form of the model equation is:

$$f = [a[(L(x))^2 - (x-0.23)^2]^{-0.5}]^{0.5} - b \qquad (4.30)$$

where: *f* - is the resonance frequency, *L(x)* - is the energy dump function, *x* - equivalent node displacement in the PM zone, *0.23* - offset factor for the operating in the PM zone, *a* - adjustable span coefficient, *b* - adjustable frequency offset. The plot of the Eq. (2.17.f) is shown again in Fig. 4.19.

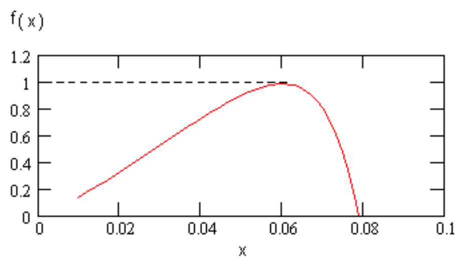

Fig. 4.19
Node resonance frequency with ZPE stabilization by the conical pendulum model

By comparing the similarity between the plot in Fig. 17 and the linear range of the plot in Fig. 4.18 we see, that they are similar with the following correspondence:

B -> x ; $(1/\nu)$ -> f.

This similarity shows, that the change of the magnetic field *B* corresponds to a linear change of the displacement *x*. In order to use the conical pendulum model for investigation the resonance frequency behaviour, we have to correct the model by taking a square root of *f*. Then the simulation equation for the resonance frequency scanning from *x* will take a form:

$$\frac{\nu_{SPM}{}^*}{\nu_{SPM}} = \left\{[a[(L(x))^2-(x-0.23)^2]^{-0.5}]^{0.5}-b\right\}^{0.5} \quad (4.31)$$

$x = k_x B$, where k_x - is a constant of proportionality.

Equation (4.31) may be used for approximative investigation of the CL node resonance frequency of the sample.

We may show, that a resonance stabilization could appear as a plateau, by using the Eq. (4.30) or (4.31). For this purpose we may simulate the dump energy as a gaussian function.

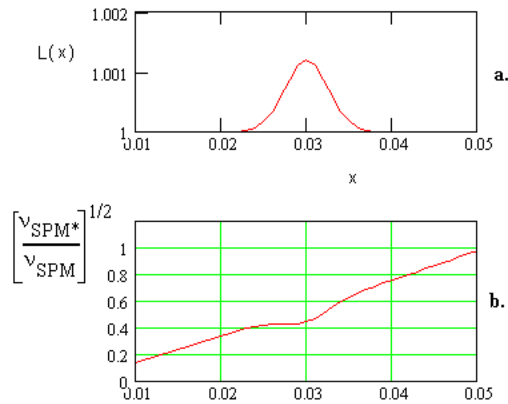

4.20
Plateau simulation by the conical pendulum model

It will correspond to the energy of some carrier when getting direct interaction from the external quantum space. The plots of the selected dump energy function and SPM frequency ratio are shown respectively in Fig. 4.20 a, b. The model does not simulate the Doppler shift, and does not provide a features for the plateau centring. But it demonstrate the mutual parameter behaviour. It also shows, that the frequency is very sensitive to the energy dumping.

In the theoretical treatment of the QHE and the provided so far data analysis, an assumption was made, that the quantum motion of the carrier in respect to the external SPM frequency corresponds to a first harmonic. If this was not true, the dependence of the observed states from B would not be arranged in a line, as the plots, shown in Fig. 4.17 and 4.18, but spread in a area. There is one additional confirmation, that the dependence of the sample SPM vector from the filling factors, and from *B* is aligned in a continuous curve. The confirmation is provided, when investigating the shift and the width of the cyclotron resonance frequency in function of the filling factor. The first successful measurements are provided by. Fig. 4.25 shows experimental data of the spectral width and shift of the cyclotron frequency in function of the filling factor at different magnetic field as a parameter.

Copyright © 2001, by S. Sarg

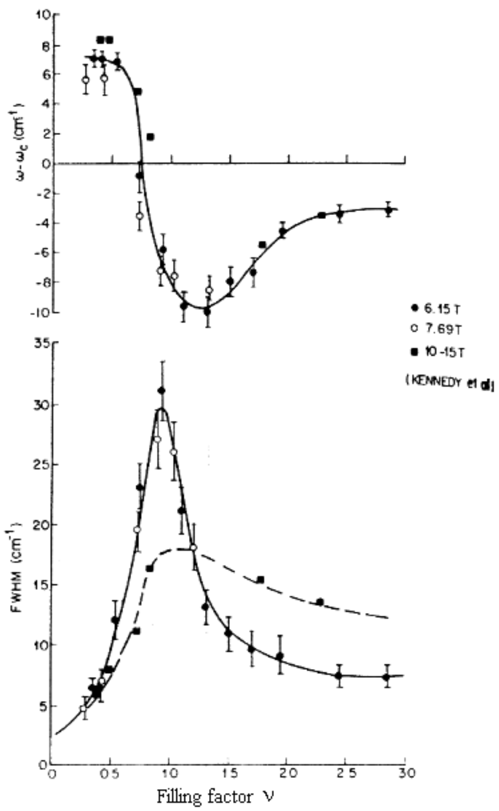

Fig. 4.21
Spectral width and shift of the cyclotron frequency in function of the filling factor (T. A. Kennedy et all. (1977)

The shift of the cyclotron frequency vs the filling factor, according to BSM means, that the SPM frequency of the sample is changed. The maximum of the cyclotron width vs the filling factor could be explained by the tendency of the different carriers to move with a same velocity, estimated as a number of passed nodes per unit time. Someone may argue, that the $\nu = 1$ state is contributes by few types of carriers: a normal electron, a single sc electron(3), a two stacked sc electron(3), and so on. However, the peak of the resonance line has a finite width. This means, that different combinations of carriers with different subharmonics numbers have a tendency to move with similar velocity. This is completely logical, if we estimate the velocity as a number of passed nodes per unit time. The node distance of the low ZPE channels is not changed by the temperature and the work for node displacement due to the FOHS motion should be a similar. So we may conclude, that:

In a low ZPE condition, the carriers tend to move with velocities closer to the optimal confined velocity of the electron.

The above conclusion is important for understanding the superconductive state of the matter.

4.4.6 The plateau width as a signature of direct interaction between the moving carriers and the quantum conditions

The plateau width for some states contributed by single and stacked SC electrons can be calculated by Eq. (4.26). The equation could be used for state combinations, whose filling factor is different of unity. Using again the experimental data of Fig. 4.11, we estimate the plateau width in B units. Then we may calculate $\Delta\nu$ by Eq. (4.26), using the data for B, p_{pr}, n_i and n^* from previous tables. In order to compare the plateau widths we have to make:

- normalization of the width to one selected value of n*

- squaring $\Delta\nu$ in order to obtain width comparison in relative units of magnetic field. (because B is under square root in Eq. (4.26).

Following this procedure a comparison between the measured and calculated plateau widths is made for some states of single and two stacked electrons. The data are presented in Table 4.4.

Table 4.4

	n*	ν	$\pm\Delta B$	ΔB_{norm}	$\Delta\nu/a_1$	$\Delta\nu_{norm}$	$(\Delta\nu_{norm})^2$
SC e-	1	1/3	1.79	3.31	27.28	2.15	4.62
SC e-	2	2/3	0.54	1	12.71	1	1
SC e-	3	3/3					
SC e-	4	4/3	0.24	0.44	7.62		
2SC e-	1						
2SC e-	2	2/5	0.93	1	23.4	1	1
2SC e-	3	3/5	0.4	0.43	14.92	0.63	0.39
2SC e-	4	4/5	0.12	0.13	8.71	0.372	0.138

The measured and calculated widths are normalised for $n^* = 2$, because this is a common available state for measuring and calculation. The accuracy of the measured plateau widths for $n^* > 1$ is significantly reduced, but our purpose is to demonstrate the procedure. The measured and calculated normalised widths from a single and two stacked electrons are combined in order to obtain the missing points for n*. Fig. 4.22 shows the re-

Copyright © 2001, by S. Sarg

sultant normalised widths plotted against the subharmonic number n*.

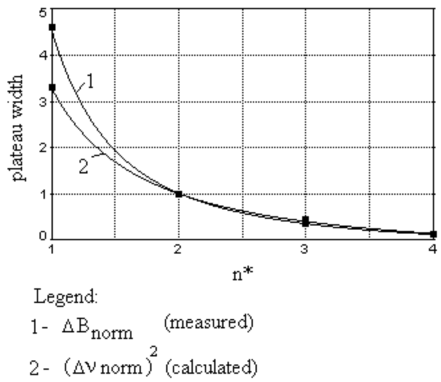

Fig. 4.22

Comparison between calculated and measured plateau widths contributed by single SC e^- and two stacked SC e^-.

We see, that some deviation exists between the theoretical and measured plateau widths for $n^* = 1$. The discrepancy could be as a result of not taking into account the following two factors:

- relative strength of the MQ boundary conditions at first harmonic
- not sinusoidal shape of MQ bumps of SPM vector.

4.4.7 Signature of the SPM vector behaviour around the critical energy level E_{c2}.

It was discussed in §4.1, that the critical energy level E_{c2}, corresponding to p. A_0 of energy well 2, can be detected by the behaviour of the SPM vector. Below the E_{c2} energy point, the SPM vector could not get 4π spatial rotation. This change of the SPM vector can be detected as disturbed quantum behaviour of the carriers. In some of the QHE experiments, this effect is observed. It is known as plateau for $B = 0$ at very low temperature or “quenching of the Hall effect”. Experimental data given in Fig. 4.14 (C. Ford et all. (1988) clearly show this effect. The plateau appears only for temperature below 100 mK and for *B* approaching zero. The plateau and the close region around the plateau, both, appear shifted from the trend of the classical Hall effect. In the same time the longitudinal resistance sharply arises, indicating a disappearance of any internal quantum effect. The strong temperature dependence of this effect is completely consistent with our theoretical considerations.

4.4.8 Signature of the positron in FQHE

The positron systems is comprised of a positive FOHS with an internal RL(T) in the trapping hole of which a negative core oscillates. According to the mass equation, and form the 1^3S_1 -2^3S_1 positronium, the proper frequency of the positron is twice the Compton frequency. Following the same logic as for the SC electron, **the positron signature in FQHE should be proportional to 1/2 state.** Such states are observed in number of FQHE experiments.

For observation of 1/2 or multiple of 1/2 state, one specific condition is important. The signatures of such states appear at much lower absolute temperature than the other fractional levels. In the experiment provided by M. P. Lilly et all. (1998), they appear, at sample temperature below 150 mK. The behaviour of the longitudinal resistance from B at different temperatures is shown in Fig. 4.23.a., b.

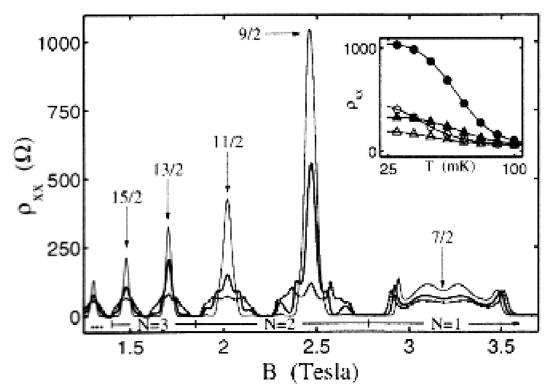

a.

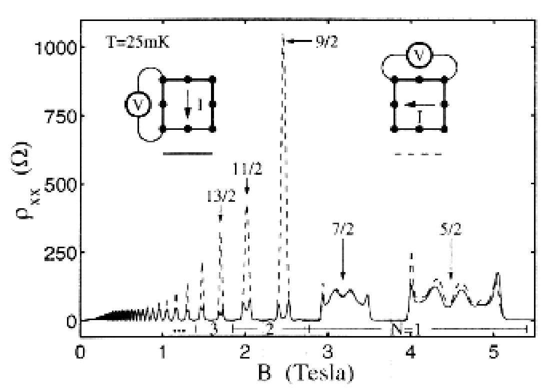

b.

Fig. 4.23

The 1/2 (and multiple) states are distinguished from integer and fractional states by a number of specific features:

- Strong peaks are observed only in the longitudinal resistance
- The observed set follows the order: 3/2, 5/2, 7/2, 9/2, 11/2,13/2,15/2.
- The plateaus of Hall resistance after 5/2 are missing
- Strong peak features appear for values above 7/2
- The peak amplitude between 7/2 and 9/2 changes with jump and then gradually decreases.
- Some anisotropy is observed when changing the direction of the current in the sample (see Fig. 4.23 b.)

Before reaching this low temperature the sample has been passed through ZPE levels (suitable for creating of SC electrons according to BSM). Let reference the analysis again to Fig. 4.3 a. At very low ZPE level, the small radius r_{min} approaches the point A. The absolute polarisation of the EQ is limited by the low ZPE. Then the proximity E-field becomes weaker and the positron could be separated from the electron shell. Due to the lower E field it could not be attracted inside of the electron. So the environment allows existence of free positrons. The free positron starts to participate in direct interactional motion due to the external quantum field. The positron charge, however is not hidden as the SC electron and may interact much stronger with some distant CL domains, which have comparatively higher ZPE. As a result of this it gets much stronger resistance. We found in the presented analysis that for all carriers, exhibiting plateau in Hall resistance, the direct interaction between them and the external SPM frequency is given by the simple relation: $\nu_{pr} = \nu_{SPM}/n_i$. This means one rotation cycle per one ν_{SPM}/n_i cycle. The n_i is additionally lowered by the much lower temperature (in comparison to QHE). Then the above condition could be satisfied only for higher axial velocity. The both factors: the larger resistance and the twice higher proper frequency (than the normal electron), are obstacles for such motion. Then the possible motion of the positron is that it may oscillate not once but number of cycles per one rotational period of ν_{SPM}. **Then the rotational frequency of the positron should be a subharmonic of** ν_{SPM}/n_i. Here again we have to keep in mind that n_i is defined only, when an internal quantum effect occurs.

One specific characteristic of 1/2 states is that the nominators are odd. This means that only the odd subharmonics are presented. But this is different in comparison to the integer and fractional QHE. The explanation of this new feature will become evident when analysing the direct interaction between the applied magnetic field and the rotating positron, interacting at subharmonic. Fig 4.24 illustrates the direct interaction due to a HD effect for three cases:

- the carrier interacts at $\nu_{pr} = \nu_{SPM}/n_i$
- the carrier interact at $4\nu_{pr} = \nu_{SPM}/n_i$
- the carrier interact at $5\nu_{pr} = \nu_{SPM}/n_i$

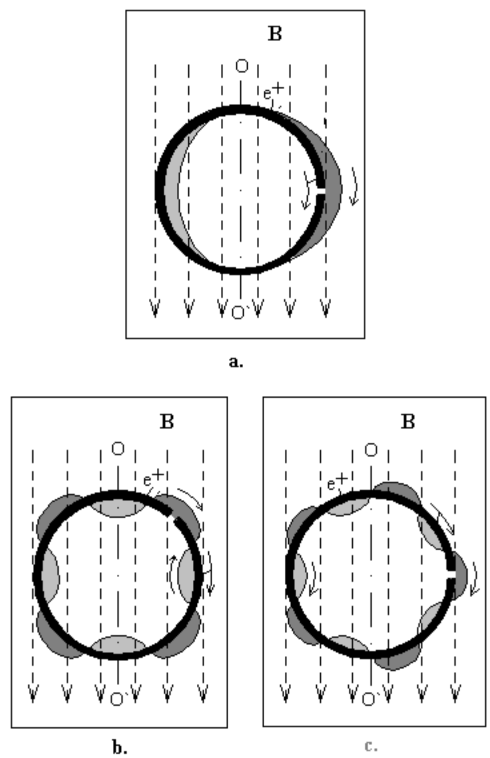

Fig. 4.24
Direct interaction between the carrier and the magnetic field for three cases (case b. does not work)

The direction of magnetic field is indicated by dashed lines with arrows and could be considered as a direction of PP SPM vector. The rotational direction of the positron ring structure is shown by arrows. The AC oscillations due to the HD effect are presented as a sinusoid around the ring. The dark shaded area of the sinosoid indicates a direction coinciding with the ring rotation, while the light shaded area is in the opposite direction. The screw type of motion due to a second order helical step assures axial motion in one direction. Due to the homogeneity of the magnetic field and carrier motion orientation, the latter takes rotational energy from the field, that is transferred to axial motion energy. The rotational energy is obtained in result of interaction between AC forces from HD effect and the PP SPM vector of the magnetic field. In order to estimate the resulting force, an axis OO‘ is drawn vertically through the centre of the positron ring. Then the interaction can be easily estimated by the balance of the forces between left and right side of the axis OO‘. The phases between PP SPM vector of B and the proper oscillations are self adjusted due to the inertial moment of the carrier from the screw type of motion.

In case **a.** the right forces are clearly predominant over the left ones. This is the HD interaction for the FQHE, discussed in the previous paragraph.

In case **b.** the right forces are equivalent to the left forces. Consequently the net effect of the ring rotation is zero. Therefore, this is a not working case. The rotation frequency is a subharmonic number four. The result is the same for all even subharmonics

In case **c.** the right forces are predominant. So this is a working case. The rotation frequency is a subharmonic number five of the proper frequency. This same situation is valid for other odd subharmonics.

Consequently, we may conclude, that:

When the direct HD interaction between the PP SPM of the magnetic field and the carriers oscillations is realised in subharmonics, the even subharmonics are excluded due to the equal balance between right and left forces.

Figure 4.24.a and b. shows two features of the peaks:

- the peak maximum has an optimum values between 7/2 and 17/2;

- the peaks are strongly dependant on the temperature

The first feature is explainable by the previous analysis. If the number of subharmonics is large, the difference between the right and the left forces will be decreased. In fact the interactional forces are not sinusoidal but possessing higher harmonics, because of the sharp bumps of the SPM MQ. The fall of the ρ_{xx} amplitude in the side of lower subharmonics number, shown in Fig. 4.23.b., could be a result of the magnetic radius dependence from the carrier velocity. At lower subharmonics the carrier motion is closer to the optimal one and the magnetic radius is smaller. Then the HD interaction also could become smaller.

The observed phenomena of the large peak change appears in a temperature range of the sample from 25mK to 100 mK. The strong dependence of the peaks from the temperature is due to the node operation at very low ZPE levels, close to E_{c2}. In order to illustrate the node operation in such conditions, the return forces - energy diagram is shown in stretched form in Fig. 4.25.

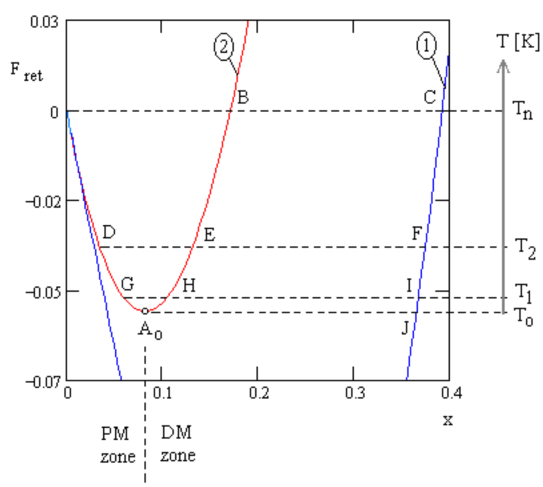

Fig. 4.25
Return forces - energy diagram by absolute temperature scale

Instead of the energy levels, the corresponding temperatures are indicated. The temperature T_n corresponds to a normal ZPE. The FQHE from electrons and SC electrons are observed in a range between T_1 and T_2. The positron signature is observed in a range between T_0 and T_1.

The small radius r_{min} for the range between T_1 and T_2 is determined by the sector HE. For operation in range T_0 and T_2, the ZPE is so small that the electrical field of the carrier RL(T) could cause enough EQ polarisation if r_{min} operates in HE sector. So the r_{min} is forced to shrink and it begins to operate in GD sector. The GD sector, however has a different sign of the slop, in comparison to the HE sector. **This affects the frequency stabilization of the synchronised quantum effect.** In such case the induced quantum effect in the sample, when interacting with the **moving and oscillating carriers** (only positrons) can not get frequency stabilization due to a Doppler effect. Now the feedback appears as a positive for the frequency stabilization, so the stabilization effect is disturbed. We have increase of the longitudinal resistance in contrary to the FQHE. The plateaus in Hall resistance are missing due to the lack of frequency stabilization.

The operation of r_{min} in the HE sector corresponds to a node operation in the PM mode, while in GD sector - to the DM mode. For lower subharmonic numbers as 5/2 and 7/2 some CL domains may operate in PM mode and others in DM mode. For this reason the both features appear; a large positive pulse (DM mode) and a small deep in the middle (PM mode). At lower temperature, more CL domains flips to DM mode.

Now let to explain the last feature - the anisotropy. When the SC electron is decayed into a positron and a degenerated electron, only the positron is an oscillation system. The degenerated electron could not participate in a quantum motion. The electrical charge of the separated degenerated electron again appears external, so it can move due to the external electrical field, but the motion is not of quantum type. From the other hand, the carriers in the external conductors (wires, power supply) are normal electrons. So in the contact points between the conductor and superconductor, the positrons and electrons has to be reconfigured in a normal electron. They both, however, had obtained different spatial distribution in the sample. When the direction of the current through the sample is changed, without changing the *B* and temperature, the old spatial distribution appears in conflict with the new required one. **This gives the effect of the anisotropy**. The anisotropy effect is also mentioned by H. L. Stormer et all, (1993).

The Landau level 1/2 in 2D at lower temperature is experimentally confirmed also by investigation the propagation of surface acoustic waves.(R. L. Willet et all. (1990). Some data from this experiment are presented in Fig. 4.26.

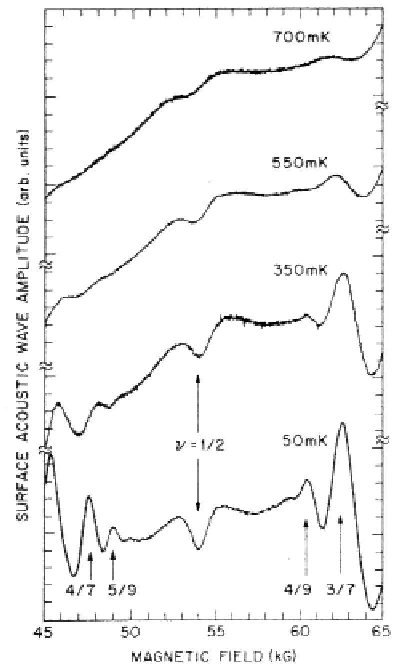

Fig. 4.26
SAW amplitude vs magnetic field at four different temperatures at 700 MHz
(courtesy of R. L. Willet et al.)

The valley in the longitudinal resistance appears only at very low temperature. This is an indication of the SC electron decay into a free positron and degenerated electron.

The signature of the free positron gives a possibility to investigate the node resonance frequency at very low temperatures. The relation between the sample and external SPM frequency is similar as those given by Eq. (4.12), but with some difference about the direct interaction

$$\nu_{SPM}^* = \frac{\nu_{SPM} p_{pr}}{n_i n'} \tag{4.31}$$

where: n‘ - is a subharmonic of the proper frequency, but indicates a different interaction.

Different notation of n‘ instead of n* is used in Eq. 4.31) in order to emphasize the different interaction. The difference is the following:

n* - denotes direct interaction, at which the n* appears a first harmonic of the external frequency between ν_{SPM} and the carrier (taking into account n_i), but in the same time is a subharmonic number of internal frequency. ν_{SPM}^*

Copyright © 2001, by S. Sarg

n‘ - denotes a direct interaction, at which n‘ appears a subharmonic of external frequency ν_{SPM} (taking into account n_i), but a first harmonic of the internal frequency $\nu_{SPM}*$.

By analogy to Eq. (4.13) for FQHE we have:

$$n_i^2 = \frac{p_{pr}}{n'} \quad \text{or} \quad n_i = \sqrt{\frac{p_{pr}}{n'}} \qquad (4.13)$$

The Eq. (4.16) $n_i = \sqrt{1/\nu}$ is also valid.

Fig. 4.27 illustrates the refractive index and the ratio (p_{pr}/n) in function of B, extracted from the data of Fig. 4.23.b. The second plot appears again linear.

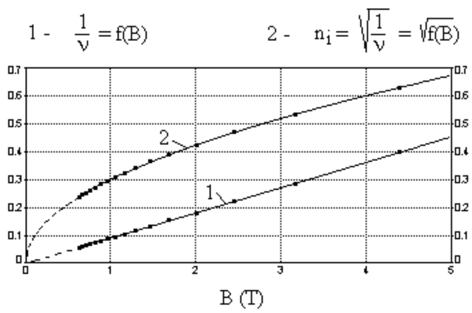

Fig. 4.27
Plot of sample refractive index and (p_{pr}/n) ratio in function of magnetic field, B

We see that the positron signature gives additional possibility to investigate the SPM frequency at very low ZPE. The refractive index at Landau level 35/2 is 0.239, but levels with higher nominators have their signature.

4.4.9 Summary and conclusions

- **The QHE gives a possibility to investigate the CL node operation at low ZPE and the quantum features of the sample space**
- **The electron system proper frequency (electron shell - positron) is equal to the Compton frequency ν_c (SPM frequency in the local Earth field).**
- **The proper frequency of the free positron system is $2\nu_c$**
- **The proper frequency of the single SC electron, is equal to $3\nu_c$, and is a same as the positron proper frequency, when it is inside the electron.**
- **The SC electrons are the carriers in the superconductive state of the matter**
- **The quantum refractive index of cooled sample may fall below unity.**
- **In low ZPE condition, the carriers tend to move with velocities closer to the optimal confined velocity of the electron**.

4.5 More about the superconductivity

After we have been acquainted with the SC state and the behaviour of charge carriers for this state, by the BSM analysis of the QHE experiments, we may try to explain one of the observed effect in the superconductors. This is the effect of long lasting current loop.

It is well known fact, that if a current is induced and allowed to flow in a closed loop inside the superconductor, it continues to flow infinitely. The necessary conditions for such state are a low temperature support and a lack of external magnetic field, which may disturb the current flow.

From the QHE experiment analysis we found, that the sample could get refractive index below unity, when CL domains with enough low ZPE are created. In §4.2.1 it was explained why the SC carriers are localised in the zone of penetration depth of the superconductor. In this zone the ZPE gradient is large. So it may always happens that some CL domains in this zone obtain a quantum refractive index equal to this of the external space (unity in air and vacuum).

$$n_i = n_{ext} = 1 \quad \text{or} \quad c* = c \qquad (4.32)$$

The depth from the surface at which the condition (43.2) is satisfied determines the penetration depth. This is illustrated in Fig. 4.28.

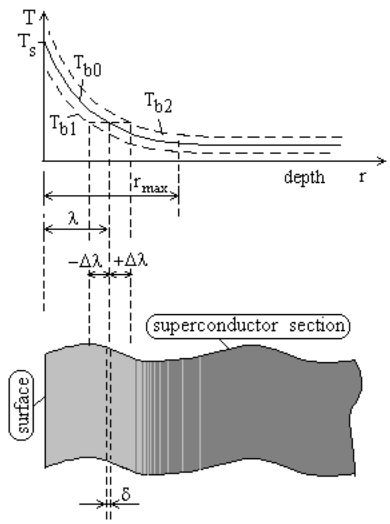

Fig.4.28
Penetration depth in function of temperature gradient and bulk temperature

The bottom part of the figure presents a transversal section of the superconductor, where the darker area corresponds to a lower ZPE and the lighter one - to a higher ZPE of the internal domains. The temperature dependence as a function of the depth, referenced to the surface at different bulk temperatures, as a parameter, is shown in the top of the figure. The shape of the curve near the surface is exponential. The relation between the three bulk temperatures is $T_{b1} < T_{b0} < T_{b2}$. The penetration depth denoted as λ, corresponds to a point of the curve in the exponential part. This gives a possibility the condition (4.32) to be satisfied for range of temperatures. In such case the penetration depth will vary with values $\pm\Delta\lambda$. The dimension of the CL domains, for which the condition (4.32) is satisfied determines the channel width δ. The channel may have not straight shape due to the hadron density nonuniformity. It however obtains a finite width, despite the exponential ZPE gradient, due to the tendency of the MQ's to congregate in magnetic protodomains. The exponential gradient of ZPE in the same time provides a direction of the induced magnetic field of the moving carrier to escape the superconductor. So **the motion of the carriers is accompanied with external magnetic field.**

It became evident, from the QHE experiments, that the carriers of the SC state are single or stacked SC electrons and they have a tendency to move with velocity corresponding to the optimal confined velocity of the electron. This means, that the single and the stacked electrons are moving with the same velocity. Due to their common interaction they moves in eshellons, as we saw by the Aharonov - Bohm oscillations. In such case, their proper oscillations are phase synchronised. This gives a strong magnetic filed, that is directed to the external space. The interaction of the moving eshellons with the sample nodes is small due to the hidden charges, but their guiding properties are preserved. In the same time the carriers carry huge intrinsic mass in their internal rectangular lattices. If we take this mass into account and apply the mass energy balance principle, we will see, that it could balance a large intrinsic energy. **This energy is mainly concentrated in the strong magnetic field in the external space around the superconductor.**

Let suppose, that the current flow velocity is deviated by some internal factor. This is equivalent to deviation of *B* from the point of the synchronised quantum effect in the QHE experiments. The large energy balance of the system “moving carriers - external magnetic filed” has enough momentum in order to return the velocity to its previous value. The stabilization mechanism involves the internal quantum effect and the automatic self adjustment of the penetration depth.

So we see, that **the induced current in the superconductor is able to flow infinitely, due to the large intrinsic energy balance.** The necessary conditions for this effect are only the lower temperature to be in a finite range and the lack of external opposing magnetic field or energy dumping.

The properties of the low energy CL domains in the superconductor will become more apparent, when the reader is acquainted with the atomic nuclear structure in Chapters 6 ,7 and 8 and its influence to the solid crystal structure.

Copyright © 2001, by S. Sarg